Theoretical Principles of Fluorescence Spectroscopy

Zuzana Limpouchová and Karel Procházka

Contents

1 Introduction 92
2 The Jablonski Diagram and Characteristics of Time-Dependent Fluorescence 93
3 Fluorescence Quenching 101
4 Resonance Energy Transfer 102
5 The Solvent Relaxation Method 106
6 Solvent Relaxation in Heterogeneous Systems 110
7 Time-Resolved Fluorescence Anisotropy 112
8 Models of Rotational Diffusion (RD) and Their Advanced Variants 114
9 Fluorescence Anisotropy in a System of Flexible Fluorescent Molecules 119
10 Rigid Molecules in Anisotropic Medium 124
11 Excimers and Exciplexes 127
12 The Effect of Ground-State Aggregation on Fluorescence Spectra 132
Appendix: Simple Quantum Mechanics Explanation of Nondegenerate Transitions Between Energy Levels in "J" and "H" Dimers 140
References 142

Abstract The chapter outlines general principles of fluorescence spectroscopy. Basic principles of radiative and nonradiative transitions (including the Jablonski diagram and Franck–Condon principle) are described and explained. The fundamentals of important fluorescence techniques, such as the steady-state and time-resolved measurements, fluorescence anisotropy, solvent relaxation method, fluorescence quenching, and nonradiative energy transfer, are discussed in detail. Special attention is devoted to the fast dynamics of individual transitions and processes influencing them at the molecular level. The end of the chapter focuses on excimers and exciplexes and mainly on the weakly bound complexes (so-called J and H aggregates), because the literature describing their behavior is relatively rare and pertinent pieces of information are not easy to find.

Z. Limpouchová (✉) • K. Procházka (✉)
Department of Physical and Macromolecular Chemistry, Faculty of Science, Charles University in Prague, Hlavova 2030, 128 40 Prague 2, Czech Republic
e-mail: zl@natur.cuni.cz; karel.prochazka@natur.cuni.cz

K. Procházka (ed.), *Fluorescence Studies of Polymer Containing Systems*, Springer Series on Fluorescence 16, DOI 10.1007/978-3-319-26788-3_4

Keywords Steady-state fluorescence spectra • Time-resolved fluorescence decays • Fluorescence anisotropy • Fluorescence quenching • Nonradiative excitation energy transfer • Solvent relaxation • Excimer • J and H aggregates

1 Introduction

Fluorescence spectroscopy is a technique that is frequently used for studying the conformation and dynamics of natural and synthetic macromolecules. This is a very versatile experimental method, which has been used in both macromolecular and colloid science and in biomedical research and also in a number of studies of low-molar-mass compounds. At present, various sophisticated fluorometers can be found among the equipment of a number of laboratories that perform polymer, biopolymer, and biomedical research (not only standard high-resolution steady-state and time-resolved apparatuses, but also fluorescent microscopes equipped with detectors and software packages that enable monitoring and analysis of multicolor time-resolved emissions from tiny polymeric nanodomains or individual organelles in living cells, etc.). The widespread use of hi-tech and simultaneously user-friendly fluorescence techniques offers new possibilities for research in various fields, but simultaneously leads to the danger of misinterpretation of the results of advanced fluorescence techniques in routine studies. Fluorescence spectroscopy is an indirect technique. The emission characteristics are influenced by an intricate interplay of different factors and should be interpreted with care and precaution. Plausible and unambiguous conclusions not only depend on profound knowledge of fluorescence principles, but almost always require additional information on the studied system provided by independent methods.

In addition to the complicated response of the fluorophore to various stimuli, one more aspect should be borne in mind. Only a small number of systems contain intrinsic fluorophores and are inherently fluorescent. Such systems (e.g., tryptophan-containing proteins) can be studied directly and reliable information on the positions, mobility, and accessibility of tryptophan residues for different molecules can be relatively easily obtained. In a majority of cases, a successful fluorescence study requires the addition of a low content of an extrinsic fluorescent probe, which modifies not only optical but also other properties of the studied system. An extrinsic probe "feels" only the effect of its immediate microenvironment, which has undoubtedly been altered by its insertion. Even though the change in the system is negligible at a macroscopic level, most fluorescence methods report the behavior of the tiny perturbed part of the system. Therefore, the extent and nature of possible perturbation of the system must also be investigated to enable description of the behavior of the unperturbed system.

The broad applicability of various fluorescence methods for investigation of both the static and the dynamic properties of different systems is based on two pillars:

1. Fluorescence is a spontaneous spin-allowed emission of a photon from the excited state, accompanied by the transition of the fluorophore to the ground state. It is a phenomenon that concerns energetically rich species (excited fluorophores) that strongly interact with the surrounding molecules and their properties (including the fluorescence characteristics) are influenced by interactions with the microenvironment. Therefore, fluorescence measurements provide useful (even though indirect) information on the host system. Because only the immediately neighboring molecules interact with the fluorophore, fluorescence techniques can be used for probing micro- and nanodomains, in which the fluorescent probe is embedded, over very short distances.
2. The excitation (absorption of a photon) and the red-shifted emission are two distinct events that are separated by a time window ranging from units to hundreds of nanoseconds depending on the fluorophore and the host system. This enables monitoring fast kinetics, because a number of molecular processes proceed on this timescale in small volumes delimited by distances comparable with the range of intermolecular interactions and affect the time-dependent emission characteristics. They include translational and rotational diffusion of the fluorophore, reorientation of molecules in the solvation shell, segmental dynamics of flexible macromolecules, and nonradiative excitation energy transfer, etc.

2 The Jablonski Diagram and Characteristics of Time-Dependent Fluorescence

It is common and convenient to discuss radiative and nonradiative transitions, as well as other processes that either lead to photochemical reactions or influence emission on the basis of the Jablonski diagram (Fig. 1), which provides a scheme of the energy levels of the electronic and vibrational states of a molecule and outlines possible routes between the states [1]. The vertical axis corresponds to increasing energy of different stable states with optimum geometry (i.e., with a minima on the energy hypersurfaces). The horizontal axis does not have any physical meaning. It is used to provide sufficient space for inclusion and description of the relevant processes. When discussing the spectroscopic characteristics of single molecules, the lines usually represent energies that can be obtained by quantum chemistry calculations in vacuum, while in condensed systems, e.g., in solutions, they represent the Gibbs free energies (i.e., potentials of the mean force) of the solvated fluorophores. The arrows (straight and curved) indicate possible transitions between different states. Typical values of the rate constants of the relevant processes are given next to the arrows.

The observation and investigation of a spontaneous emission of photons from a macroscopic sample assumes the excitation of a certain fraction of molecules to higher electronic energy states. Excitation can be achieved by different means (absorption of light, excitation energy transfer, chemical reaction, etc.). This part

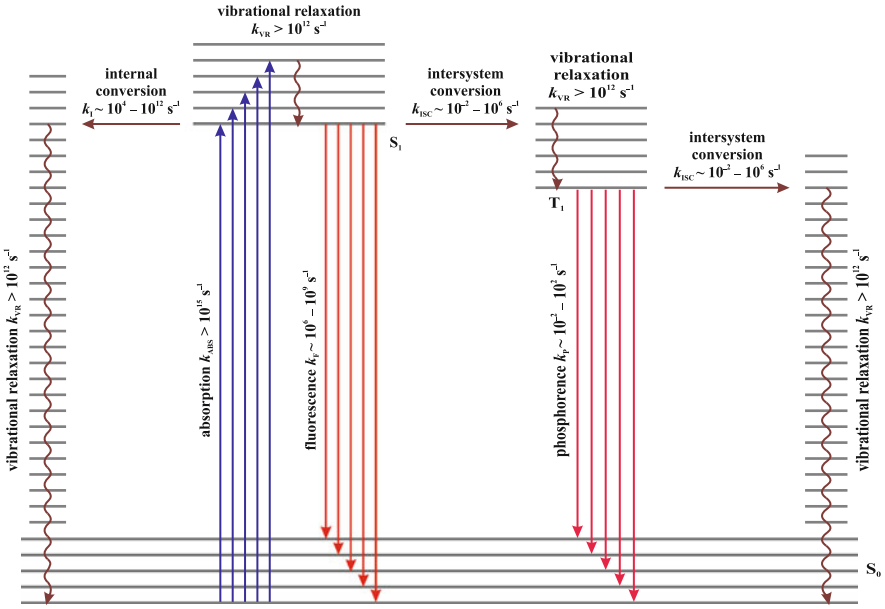

Fig. 1 Jablonski diagram: the energies of the ground electronic singlet state S_0, excited singlet S_1, and triplet T_1 (together with relevant vibrational states) are depicted by *horizontal lines*; the most important optical and nonradiative transitions are depicted by *arrows* and *wavy lines*, respectively; the typical values (in orders of magnitudes) of rate constants of the processes have been also included. Adapted from Springer, Self Organized Nanostructures of Amphiphilic Block Copolymers I, 241, 2011, 187–249, figure 1, [2]. Copyright 2011. With kind permission from Springer Science and Business Media

of the review focuses on the spectroscopic process (absorption of photons), which assumes irradiation of the sample by incident light of an appropriate wavelength. Under the current conditions of spectroscopic measurements, which employ fairly weak excitation light intensity, only a low fraction of the molecules of the fluorophore (less that 10^{-6}) interact (collide) with passing photons, absorb them, and become excited. Before discussing emission from a macroscopic sample, we will analyze all the processes that can occur at the level of a single molecule.

We will concentrate on the behavior of common fluorophores at ambient temperatures, i.e., on molecules with fully paired spin only of the valence electrons, i.e., we will not discuss the photophysical behavior of radicals, biradicals, etc. Under ambient conditions, the fluorophore occurs in the lowest vibrational state of the lowest electronic state (ground state, S_0). The probability of absorption of a photon is proportional to the square of the transition dipole moment (which, to a first approximation, represents the difference between the dipole moments in the excited and ground states). It is convenient to formulate the optical selection rules which summarize the roles of several important factors [3–5]. The most severe restriction concerns the spin. Within the Born–Oppenheimer approximation, which postulates that the slow motion of nuclei can be (from a mechanistic point of view) separated

from the fast motion of electrons, the spin must be conserved. In the opposite case, the transition is strictly forbidden. In reality, the spin–orbit interaction in molecules containing atoms with several valence electrons (carbon, nitrogen, oxygen, etc.) relaxes this selection rule and, in addition to spin-allowed transitions (fluorescence), also singlet–triplet and triplet–singlet transitions (intersystem crossing) can be observed in some systems. In the latter case, the radiative transition is called phosphorescence. However, the probability of intersystem crossing is very low. It is weakened by a factor of ca. 10^{-5}–10^{-7} in comparison with a fully allowed transition. The second restriction concerns the symmetry of the wave functions of states involved in the transition. As the transition dipole moment operator is antisymmetric and its product with the wave functions of both states must be symmetric to yield a nonzero value after 3D integration over the space, a strictly symmetry-allowed transition can occur only between two states described by symmetric and antisymmetric wave functions (or vice versa). Nevertheless, antisymmetric vibrations can relax the symmetry selection rule and various "forbidden" transitions (weakened only by a factor of 10^{-1} to 10^{-3}) can be observed in a number of systems (e.g., some strong bands in the fluorescence spectra of condensed aromatic molecules, such as naphthalene, anthracene, etc., are, strictly speaking, symmetry-forbidden transitions and occur only thanks to antisymmetric vibrations). The last condition concerns the overlap of wave functions: a large value of the transition dipole moment (difference between the dipole moments in the two states) requires the redistribution of the cloud of electrons during the transition, but the electronic wave functions of both states should acquire nonzero (preferentially large) values in the same places, i.e., the wave functions must overlap reasonably in space to yield a nonzero value after the integration of their product with the transition dipole moment operator. The overlap of the ground and exited wave functions differs from one fluorophore to another and the weakening factor ranges from 10^{-1} to 10^{-5}; e.g., the $n \rightarrow \pi^*$ transition (absorption) in compounds containing an aliphatic carbonyl group involves a transition from the non-bonding orbital localized on the oxygen atom to the antibonding orbital localized mainly on the carbon atom—in this particular case, the overlap is small and the absorption is weak in spite of considerable redistribution of electrons.

The transition of a molecule to a higher excited state due to the absorption of a photon is one of the fastest processes on Earth. It is accomplished in times shorter than 10^{-15} s. No chemical process can proceed with a comparable speed and only a few nuclear processes, which occur over extremely short length scales of 10^{-15} m, are faster. This means that the transition proceeds adiabatically without interaction of the fluorophore with the microenvironment and there is no change in either the positions of the nuclei of atoms forming the fluorophore or in the arrangement of the surrounding molecules. It follows that the molecule retains the ground-state geometry immediately upon excitation. The consequences of the high transition speed can be easily illustrated for a diatomic molecule (see Fig. 2). In this case, the energy of the states depends only on the distance between the two nuclei and can be expressed by the Morse function. A detailed energy scheme can be appropriately depicted in 2D representation and individual photophysical processes can be

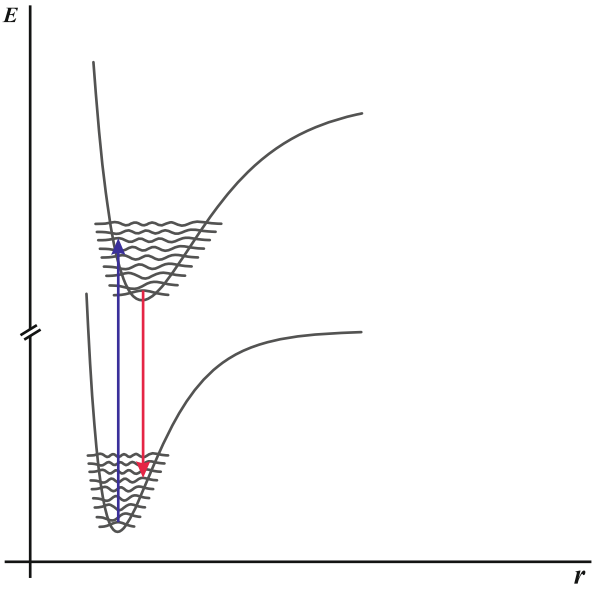

Fig. 2 The Franck–Condon principle: the energies of the ground and the first excited singlet states, S_0 (*lower curve*) and S_1 (*upper curve*), respectively, of a diatomic molecule are presented as functions of the distance between atoms, *r*. Several vibration wave functions (*note*: the probabilities of interatomic distances are proportional to the square of the corresponding wave functions) are also depicted. The *vertical arrows* stand for the most probable absorption and emission.

comprehensively discussed and simply explained. The lowest curve shows the energy of the ground state (vertical axis) as a function of the separation of the two nuclei (horizontal axis). The horizontal wave lines depict several selected vibrational states. The grey curves show the corresponding wave functions (note that the geometry of the molecule with a given separation of nuclei is proportional to the square of the corresponding wave function value for this distance). The curve corresponding to the bonding excited state is shifted to the right because the excited (energetically richer) bimolecular molecule is generally larger.

At ambient temperatures, the ground-state molecule occurs in the lowest vibrational state and the most probable distance between the nuclei r_E lies close to the position of the minimum of the lowest Morse curve. As the distance of the nuclei does not change during excitation, it is evident that the absorption of a photon generates not only electronically, but also vibrationally excited states (to satisfy the condition of sufficient overlap of the vibrational wave functions of the two states—the Franck–Condon principle [6, 7]—see Fig. 2).

The most probable transitions are depicted by the upward pointing vertical arrows. Upon excitation, the molecule tries to get rid of the excess energy as fast as possible. The fastest process possible in condensed media (although slower by several orders of magnitude than the absorption) is vibrational relaxation. This is a nonradiative process and it proceeds in most nonviscous solutions on timescales of 10^{-14} to 10^{-12} s. The excess energy (of excited vibrations) is rapidly and efficiently transferred to the surrounding medium during collisions with neighboring molecules, because the masses of the colliding particles are comparable and the frequency coincides with the frequency of intermolecular collisions. After the

vibrational relaxation, the excited molecule ends up in the lowest vibrational state of the electronic excited state and then the emission of a photon, i.e., radiative transition to the ground state (fluorescence) can occur. However, a number of fast nonradiative processes compete with fluorescence. They will be discussed later.

The probability of the spin-allowed $S_1 \rightarrow S_0$ emission of a photon (fluorescence) depends, similarly to the absorption probability, on a change in the dipole moment during the transition and on the energy difference between the states. For a fully (spin, symmetry, and overlap) allowed transition, the quantum mechanics calculation yields a rate constant of about 10^9 s^{-1}. This means that the natural mean lifetimes of the excited state of common fluorophores are nanoseconds. The real lifetimes of a number of important fluorophores can be longer (tens to hundreds of nanoseconds) if the transition is not fully allowed, but it can be much shorter (in the picosecond range) if nonradiative processes efficiently deplete the excited state. In both cases, the normalized fluorescence intensity (number of photons emitted per second from a unit volume of a macroscopic ensemble of fluorophores normalized by a number of incident photons passing this volume) is weaker than expected. In an overwhelming majority of cases (flexible molecules strongly interacting with the surrounding medium), the nonradiative depletion of the excited state quenches the fluorescence completely and only a small number of rigid molecules (e.g., condensed aromatic rings) are fluorophores of practical use. It is necessary to realize that, regardless of the actual lifetime of the excited state, the single act of emission of a photon and the $S_1 \rightarrow S_0$ transition proceed in times of ca. 10^{-15} ns and the ground-state fluorophore ends up in a vibrationally excited state (see Fig. 2, where the emission is depicted by the downward pointing arrows). Then a fast vibrational relaxation takes place on a ps timescale and the fluorophore returns to its lowest possible energetic state, which (together with vibrational relaxation after the excitation) explains the intrinsic Stokes shift of the emission towards the red part of the spectral region with respect to the absorption wavelength [8].

Because both the absorption and emission proceed between states S_0 and S_1 and their probabilities depend on the same dipole moments, it is not surprising that there is (in most cases) a linear relationship between the molar absorption coefficient and the rate constant of the spontaneous emission (the higher the absorption probability, the higher the emission intensity). However, because the competing processes often deplete the excited state faster than fluorescence, the observed emission intensity is usually considerably weaker than expected. The relationship between the absorption coefficients of $S_0 \rightarrow S_i$ excitations ($i \geq 2$) and the rate of $S_1 \rightarrow S_0$ emission is not straightforward. If the molecule is excited to higher electronic states S_2, S_3, etc., in an overwhelming majority of cases, the excited molecule reaches the lowest vibrational level of the lowest excited S_1 state by a cascade of vibrational relaxation processes on a ps timescale before the emission of a photon occurs. There are only a few exceptions from the rule postulating that the emission always proceeds from S_1, e.g., azulene [9] exhibits fluorescence from S_2.

So far we have considered various processes at the level of only one molecule. However, fluorescence spectroscopy is used for studying macroscopic samples. Thus, the emission of photons from a large number of excited fluorophores is

monitored and analyzed (except for single-molecule fluorescence spectroscopy and fluorescence-correlation spectroscopy). Under current spectroscopic conditions, the concentration of fluorophores is usually low (typically 10^{-6}–10^{-5} mol L^{-1}) and the intensity of the irradiation is fairly weak. Hence, only a small fraction of the fluorophore molecules are excited, typically less than 10^{-6}, but this still represents a large ensemble of 10^9 excited molecules per milliliter. Therefore, it is necessary to discuss the kinetics of depletion of excited states in a large (macroscopic) ensemble of fluorophores. The depletion of excited states is a stochastic process that involves a number of independent competing contributions (internal conversion, intersystem crossing, etc.). The probabilities of the individual processes depend on the chemical nature of the fluorophore and on its interaction with its microenvironment [10]. Individual processes will be discussed later.

First, we will describe the fluorescence kinetics after excitation with an ultrafast excitation pulse that can be approximated by a δ-pulse in the absence of nonradiative processes that could deplete the excited state (idealized case of time-resolved fluorescence decay measurements) [11, 12]. In a system of equivalent fluorophores (embedded in a homogeneous medium and interacting equally with the microenvironment), all the excited molecules have the same probability of emission of a photon but, due to the stochastic nature of the spontaneous emission, only the relationships concerning large numbers of fluorophores can be formulated. It is obvious that the number of photons released per unit time (rate of emission, or fluorescence intensity, $F \propto dN_F/dt$) in the system without competing nonradiative processes equals the total rate of de-excitation (depletion of the excited state), $-dN/dt$, which is proportional to the number of fluorophores excited at a given time, $N(t)$. Hence, we can write: $-dN/dt = k_R N(t)$, where k_R is the rate constant of the radiative transition (in this case, it is the rate constant of fluorescence, k_F). Integration yields kinetics that obeys the single exponential decay (first-order kinetics), i.e.,

$$N(t) = N_0 \exp(-k_R\ t), \quad \text{or} \quad F(t) = F_0 \exp(-k_R\ t), \tag{1}$$

where N_0 or F_0 is the number of excited molecules or fluorescence intensity, respectively, immediately upon excitation. In a great majority of practically important cases, the experimental decay is not single exponential because either the underlying photophysics is more complicated or the fluorophores embedded in a nonhomogeneous medium are not equivalent (individual fluorophores interact differently with their microenvironment). In almost all cases, some nonradiative processes compete to a certain extent with fluorescence. They contribute to the depletion of the excited state upon excitation and the fluorescence is weaker and decays faster. In this case, the experimental rate constant k_{exp} is the sum of the rate constants k_i of all the processes depleting the excited state (including the radiative process), $k_{exp} = \Sigma k_i$. The fluorescence quantum yield (the ratio of the number of emitted photons N_F to the number of absorbed photons N_{abs}), $\Phi_F = N_F/N_{abs}$, is lower than one (given by the relationship $\Phi_F = k_R/\Sigma k_i$) and the fluorescence intensity is weaker; it is attenuated (with respect to the ideal value) by the same factor $k_R/\Sigma k_i$.

The fluorescence lifetime is defined as the time at which the intensity of emission decays to $1/e$ of its initial value, i.e., $\tau_F = 1/k_{exp}$.

As was explained above, a number of nonradiative processes can deplete the excited state and quench the fluorescence. The first common process is internal conversion, IC. Its probability depends on the structure and properties of the molecule and on interaction with the surrounding molecules, and its rate varies over a wide range of orders of magnitude. For flexible and strongly interacting molecules, IC can proceed on a picosecond timescale and can efficiently deplete the excited state before considerably slower emission takes place. This process actually means that most molecules are nonfluorescent and only a relatively small number of rigid molecules are strong fluorophores. This also explains why the fluorescence intensity decreases with increasing temperature, with increasing polarity of the solvent and with its decreasing viscosity.

The second important nonradiative process is $S_1 \rightarrow T_1$ intersystem crossing, ISC, which is strictly forbidden by the spin selection rule at the level of the Born–Oppenheimer approximation, but the selection rule is relaxed in real systems by spin–orbital interaction for almost all the molecules that contain atoms with more electrons. The easiness of ISC depends on the energy difference between states S_1 and T_1 and, for molecules with energetically close S_1 and T_1 states, this process can be very fast and efficient (k_{ICS} ca. 10^{12} s^{-1}) due to the resonance effect and intermixing of the S_1 and T_1 states, while it practically does not come into account for molecules with a large energy difference. If the $S_1 \rightarrow T_1$ transition takes place, the molecule occurs in an unenviable situation. The probability of the radiative $T_1 \rightarrow S_0$ transition (phosphorescence) is low because the process is spin forbidden and the energy difference between the states is large. The molecule contains a considerable amount of excess energy and therefore is very reactive and on average remains in the reactive state for quite a long time and undergoes a number of collisions with the surrounding molecules. Therefore, the probability of photochemical reaction (i.e., the transformation of the original molecule in another one) is high and most photochemical reactions involve molecules (reactants or photosensitizers) in the excited T_1 state. Because the energy of the T_1 state is lower than that of the S_1 state, the phosphorescence is red shifted with respect to the fluorescence. Its intensity is very low due, in part, to its low natural rate (rate constant k_P ca. 10^{-3} to 10^3 s^{-1}) and to competitive depletion of the excited state by vibrational relaxation, collision energy transfer, etc.

If states S_1 and T_1 are energetically close, the molecule can "escape" from the T_1 state and return to the S_1 state. It is obvious that the T_1 molecule must gain some energy to reach the level where the energies of states T_1 and S_1 overlap. The required excess energy can be generated by intermolecular collisions with the surrounded molecules or by triplet–triplet annihilation, which requires interaction of two excited species. In both cases, delayed emission from S_1 occurs. The first mechanism is called delayed fluorescence of type E (because eosin is an important molecule which exhibits this type of delayed fluorescence) and the second mechanism is referred as type P (according to pyrene). In both cases, it is a slow radiative

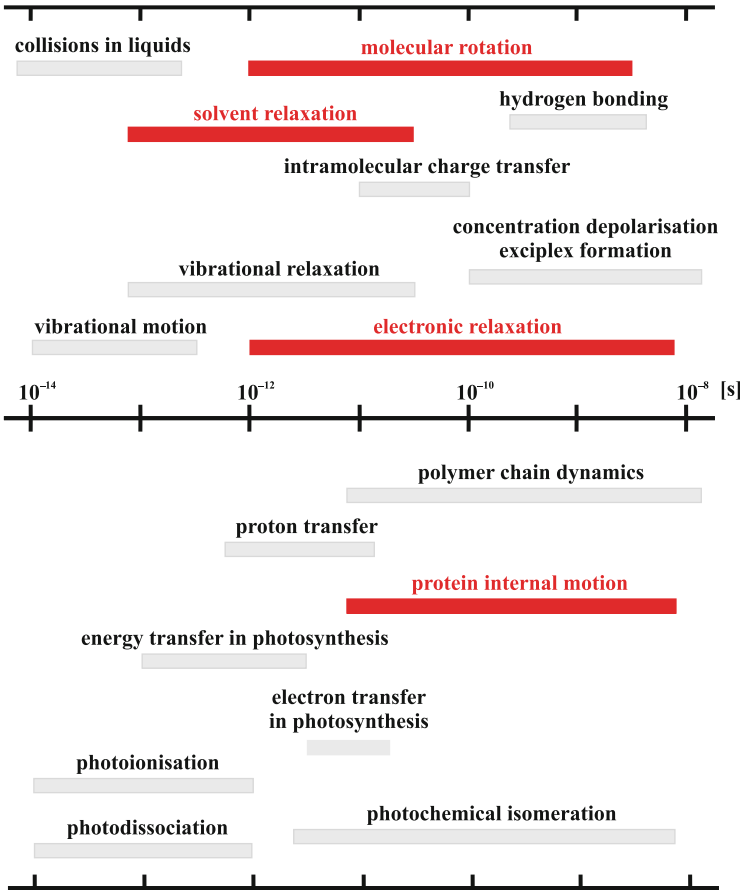

Fig. 3 The outline of fast dynamic processes that proceed at rates comparable with that of the radiative depletion of the excited state and can be studied by time-resolved fluorescence techniques (TRF): the rate of the polymer chain dynamics (vibrational motion and relaxation) strongly overlaps that of electronic relaxation and can be studied by TRF. Adapted from Springer, Self Organized Nanostructures of Amphiphilic Block Copolymers I, 241, 2011, 187–249, figure 3, [2]. Copyright 2011. With kind permission from Springer Science and Business Media

process with low intensity. In the first case, the rate constant equals that of phosphorescence, i.e., k_P; in the second case it equals $½k_P$.

The advantage of fluorescence measurement for studying the dynamic behavior of various systems follows from the fact that a number of processes can occur in the time window between absorption and emission. Either the fluorophore itself can undergo some changes (transition between electronic states, conformational changes, changes in position due to rotational or translational diffusion) or the surrounding molecules can reorganize (solvent relaxation, close approach of quenchers, etc.). Figure 3 gives a survey of practically important dynamic processes that proceed at rates comparable with fluorescence, affect the fluorescence

characteristics (position, width and shape of the fluorescence spectra, quantum yield, decay time, etc.), and can be studied by time-resolved fluorescence spectroscopy (TRFS). Some of them, which play an important role in fluorescence studies of polymer dynamics, conformations, and assembly, will be discussed in detail in the following text.

3 Fluorescence Quenching

All nonradiative processes that contribute to the depletion of the excited state shorten the fluorescence lifetime and weaken the emission intensity. Some of them arise as inherent features of the fluorophore (e.g., internal conversion) and their effect depends on its interaction with solvent and on temperature. They predetermine the natural fluorescence lifetime, τ_{F0}, which is defined as the lifetime in the absence of additional components that can quench the fluorescence.

Compounds that strongly interact with an excited fluorophore and quench its fluorescence are called "quenchers." Efficient quenching requires close approach of the quencher to the fluorophore, which means that a fluorescence quenching study yields information on a tiny volume element in which the fluorophore is embedded and on the processes that proceed in its vicinity. Hence, it can be used for probing tiny nanodomains of the system. Fluorescence quenching experiments are usually not difficult from the experimental point of view and they have often been used in biochemistry and polymer science since the early 1950s [13]. In homogeneous bulk solutions, the time-resolved data provide information on the rate of diffusion; in nanoheterogeneous systems with specifically embedded probes (e.g., covalently attached to the polymer chain), they can answer the question of whether a particular domain is accessible to the particular (polar or nonpolar) quencher, i.e., if the domain itself is polar or nonpolar.

Fluorescence quenching processes can be divided into two main categories: (1) dynamic (collision) and (2) static quenching. In the first case, the quencher (usually a transition or heavy metal ion or its complex, a molecule containing a heavy atom, or just oxygen dissolved in the solution) collides with the fluorophore and the excitation energy is transferred to the quencher and later dissipated in the surrounding medium. This quenching mechanism contributes to the depletion of the excited state, shortens the fluorescence lifetime, and weakens the fluorescence intensity. Both the fluorescence intensity F and lifetime τ_F obey the well-known Stern–Volmer relation [14].

$$\frac{F_0}{F} = \frac{\tau_{F,0}}{\tau_F} = 1 + K_{SV} c_Q \tag{2}$$

where the symbols without and with subscript $_0$ apply to the system with and without quencher, respectively, K_{SV} is the Stern–Volmer quenching constant which can be expressed as a product of the dynamic quenching rate constant k_q

and the fluorescence lifetime in the absence of the quencher, $\tau_{F,0}$, and c_Q is the concentration of the quencher. Detailed mechanism is relatively complicated and involves several steps. If we assume only free diffusion of both the fluorophore and quencher in the bulk solution and neglect the transient terms, k_q is a product of the quenching efficiency, which depends on the fluorophore–quencher pair, and the diffusion-limited bimolecular collision rate constant, k (defined by the Smoluchowski equation, $k = 4\pi D_s R_s N_A$, where D_s and R_s are the sum of the effective diffusion constants and the molecular radii of the components, respectively, and N_A is the Avogadro number).

Static quenching does not assume diffusion of components. It is a result of the reversible formation of a nonfluorescent fluorophore–quencher complex in the ground state. A fraction of the fluorophore is bound in a complex and makes no contribution to the emission, but the remaining fraction is not affected and exhibits fluorescence with the natural lifetime, $\tau_{F,0}$. The emission intensity is weaker and obeys the Stern–Volmer plot

$$\frac{F_0}{F} = 1 + K_A c_Q \tag{3}$$

where K_A is the association constant describing the reversible formation of the complex and where the fluorescence lifetime is not affected by the presence of the quencher. A combination of steady-state and time-resolved measurements allows unambiguous discrimination between the different types of quenching. Moreover, the static and dynamic quenching mechanisms differ significantly in the temperature dependence of their efficiency. Increasing temperature accelerates diffusion and amplifies dynamic quenching but promotes the dissociation of the complex and restricts static quenching. Hence K_{SV} (and the slope of Stern–Volmer plot) increases and K_A (and the slope) decreases with temperature.

In some real systems, it is possible to encounter a combination of both types of quenching. The Stern–Volmer plots are frequently not linear because various transient effects may cause the upward curvature of the plot. On the other hand, downward curvature and leveling-off of the plots can be a result of uneven (hindered) accessibility of a fraction of fluorophores in micro-heterogeneous media. A number of specific models for analyzing fluorescence decays affected by quenching have been proposed in the literature [8, 15].

4 Resonance Energy Transfer

The fluorescence resonance energy transfer (FRET), also called nonradiative excitation energy transfer (NRET) or direct energy transfer (DET), is one of the processes that quench the fluorescence of an excited fluorophore. In contrast to collision quenching, the excitation energy of the donor is transferred to another molecule (acceptor) over nanometer distances and the underlying mechanism does

not require the close contact of interacting species. When the energy is transferred, the originally excited donor returns nonradiatively to the ground state and the acceptor becomes excited. The acceptor can be a practically important fluorophore, which then exhibits its characteristic fluorescence, or a molecule that is efficiently deactivated by a nonradiative internal conversion. Analogously to collision quenching, NRET is a widely used fluorescence variant that has been employed in polymer and colloid science since the middle of the twentieth century. The FRET mechanism was first elucidated by Förster more than 60 years ago. It assumes a "long-range" interaction of the dipole moment of the excited donor with the dipole moment of the ground-state acceptor (in the nanometer range). The orbitals of the two species do not overlap and the resonance mechanism of weakly coupled dipoles controls the rate of the transfer. Efficient energy transfer requires approximately the same or slightly lower energy of the excited acceptor than that of the donor, because some excess energy can be dissipated in vibrational energy. From the spectroscopic point of view, the condition of total energy conservation means that the absorption spectrum of the acceptor has to overlap with the emission spectrum of the donor. The greater the overlap, the more efficient and faster is the energy transfer. The theory [16–18] predicts a steep dependence of the transfer rate constant, k_T, on the distance between the donor and the acceptor

$$k_T = \frac{1}{\tau_D}\left(\frac{r_0}{r}\right)^6 \tag{4}$$

where τ_D is the fluorescence lifetime of the donor in the absence of the acceptor and r_0 is the Förster radius, defined as the critical donor–acceptor distance for which the rate of fluorescence emission of photons (in a macroscopic sample) and energy transfer are the same. At the level of a single donor–acceptor pair, this means that, if the molecules are separated by r_0, the probability of emission of a photon from an excited donor is the same as that of resonant energy transfer. As already indicated, r_0 depends on the overlap of the emission and absorption spectra of the donor and acceptor, respectively. The normalized overlap integral J is defined by the following formula

$$J = \frac{\int F_D(\lambda)\varepsilon_A(\lambda)\lambda^4 d\lambda}{\int F_D(\lambda)d\lambda} \tag{5}$$

where $F_D(\lambda)$ and $\varepsilon_A(\lambda)$ are the emission spectrum of the donor and molar absorption coefficient of the acceptor as functions of the wavelength λ, respectively. However, the Förster radius also depends on the mutual orientation of the dipoles (expressed by the orientation factor, κ) and on the fluorescence quantum yield of the donor in the absence of the acceptor, Q_D. The complete formula reads

$$(r_0)^6 = \frac{9(\ln 10)\kappa^2 Q_D J}{128\pi^5 n^4 N_A} \tag{6}$$

where n is the refractive index and N_A is the Avogadro number. This formula shows that the larger the overlap, the larger is the region of efficient interaction and longer is r_0. If the current chemical units are used, i.e., $(\text{mol/L})^{-1}\,\text{cm}^3$ for the absorption coefficient, and cm for the wavelength, then the value of $(r_0)^6$ can be enumerated (in Å) using the following mathematical prescription: $r_0 = 9.78 \times 10^3 (n^{-4} Q_D \kappa^2 J)^{1/6}$.

The transfer efficiency, E, is defined as the ratio of the transfer rate constant, k_T, to the sum of rate constants, k_i, of all the processes that deplete the excited state (radiative and nonradiative, i.e., including the rate of unaffected fluorescence and that of FRET, k_T and k_F, respectively), $E = k_T/\sum k_i$. Experimentally, E can be determined by measurement of the quantum yields (or fluorescence intensities of the donor in the presence and absence of the acceptor, F_{DA} and F_D, respectively, or by time-resolved measurement of the corresponding fluorescence lifetimes, τ_{DA} and τ_D). If the acceptor is fluorescent (which is not a necessary condition), its emission can also be used for evaluation of E. However, the latter approach is not often used and its precision is usually lower (because the acceptor intensity can be affected by a number of complicating factors and also direct acceptor excitation contributes to its emission):

$$E = 1 - \frac{F_{DA}}{F_D} = 1 - \frac{\tau_{DA}}{\tau_D} = \frac{\varepsilon_{AD}(\lambda_1)}{\varepsilon_{DA}(\lambda_1)} \left(\frac{F_{AD}(\lambda_2)}{F_A(\lambda_2)} - 1 \right) \tag{7}$$

where $\varepsilon_{AD}(\lambda_1)$ and $\varepsilon_{DA}(\lambda_1)$ are the absorption coefficients of the donor and acceptor, respectively, at the wavelength of the absorption, λ_1, in the sample containing both donor and acceptor and $F_A(\lambda_2)$ and $F_{AD}(\lambda_2)$ are the fluorescence intensities of the same concentrations of acceptor at λ_2 in the absence and presence of the donor, respectively, both excited at λ_1 and monitored at λ_2.

The orientation factor between fixed dipoles is given by

$$\kappa^2 = (\cos\vartheta_T - 3\cos\vartheta_D \cos\vartheta_A) \tag{8}$$

where ϑ_T is the angle between the donor emission dipole and the acceptor absorption dipole, and ϑ_D and ϑ_A are the angle between the vector joining the donor and the acceptor and the corresponding dipoles, respectively. The factor κ^2 ranges from 0 for perpendicular orientation to 4 for parallel orientation of the dipoles. However, in solutions, the fluorophores are randomly oriented and undergo fairly rapid rotational diffusion. For very fast rotation in an isotropic, low viscosity solvent, when the molecules assume all mutual orientations with equal probability, time and ensemble averaging yields the "fast dynamic random limit" $\kappa^2 = 2/3$.

Nonradiative excitation energy transfer affects the time-resolved fluorescence decay and shortens the experimental values of the average fluorescence lifetime of the donor. In a macroscopic system, the shape of the decay curve depends on the

spatial distribution of the quenchers with respect to the donors and the time-resolved measurements can be used for studying the distribution and motion of the quenchers in complex systems. Early theoretical works [16, 19] were focused on isotropic systems with randomly distributed fluorophores and quenchers. In such systems, all fluorophores are influenced evenly by surrounding quenchers and the average number of quenchers in a thin spherical layer with radius r around each donor is proportional to r^2. The decay rate in a macroscopic system of fluorophores and quenchers can be generally obtained as the solution of the stochastic master equation which describes the time derivative of the average probability $\langle \rho(t) \rangle$ that the excitation at time t is still localized at the same fluorophore which was excited at time $t = 0$. The derivative gives the rate of deactivation of the excited fluorophores and (similarly to other common stochastic processes) is proportional to the number of excited fluorophores at a given time, i.e., $d\langle \rho(t) \rangle / dt = - k_{\text{exp}} \langle \rho(t) \rangle$. The effective rate constant depends on the spatial distribution of the quenchers with respect to the fluorophores

$$k_{\text{exp}} = \frac{1}{\tau_{\text{D}}} + \frac{1}{\tau_{\text{D}}} \sum_{k=1}^{N} \left(\frac{r_0}{r_k} \right)^6 = \frac{1}{\tau_{\text{D}}} + \frac{1}{\tau_{\text{D}}} \int W(r) \left(\frac{r_0}{r} \right)^6 dr \tag{9}$$

where r_k are the distances of the quenchers from a randomly chosen fluorophore and $W(r)$ is the distribution function of the numbers of quenchers at a distance r (in a random mixture proportional to r^2). Solution of the differential equation $-dN/dt = k_{\text{exp}} \cdot N(t)$, or $-dF_{\text{DA}}/dt = k_{\text{exp}} \cdot F_{\text{DA}}(t)$, with k_{exp} given by Eq. (9) and $W(r)$ proportional to r^2 yields the following time-resolved decay of the fluorescence intensity, $F_{\text{DA}}(t)$:

$$F_{\text{DA}}(t) = F_0 \exp\left[-\left(\frac{t}{\tau_{\text{D}}} \right) - 2\left(\frac{c}{c_0} \right) \sqrt{\frac{t}{\tau_{\text{D}}}} \right] \tag{10}$$

where c_0 is the critical concentration, $c_0 = 3000/(2\pi^{3/2} N_{\text{A}} r_0^3)$. The derived equation has been checked experimentally and was found to describe the experimental decays reasonably well. When the fluorophores and quenchers are embedded in small volumes, the decays must be described by more complicated relationships. The complication derives from the fact that individual fluorophores, which are located at different places with respect to the center of the closed volume element or in volumes differing in size, are surrounded by different numbers of quenchers and cannot be considered to be equivalent probes, e.g., those located close to the walls are affected only from one side, while those in the middle are affected on average by a spherically symmetrical set of quenchers (see Fig. 4). The NRET effect in small volumes was studied by Fayer and independently also by Winnik and appropriate formulas have been proposed and tested [20–25] and they will be discussed in the next chapters.

Fluorescence quenching and FRET belong among very popular and frequently employed fluorescence variants. They have been widely used in various fields

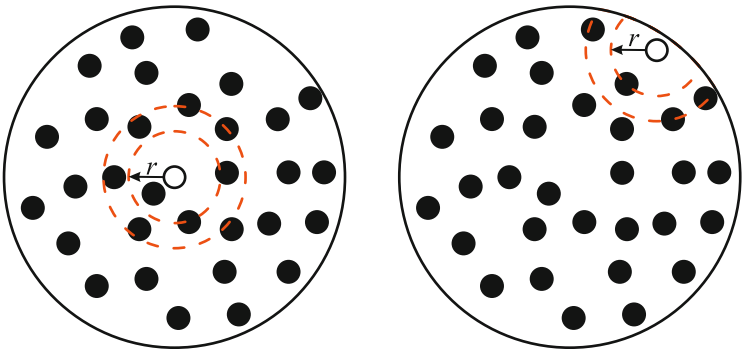

Fig. 4 Distribution of acceptors around a donor in small restricted volumes; the figure shows the importance of the location of the donor in confined and spatially restricted systems

including polymer and biopolymer research. FRET has been used in studies of polymer miscibility [26, 27] and polymer chain conformations [28–30]. Collision quenching, which provides information on the accessibility of fluorophores embedded in heterogeneous materials for different quenchers, has been used to study the properties of nanodomains, etc. [2, 31–34]. Both methods represent classical "benchmark" fluorescence techniques in polymer science. Their specific use for studies of polymer conformations, dynamics, and self-assembly will be discussed in detail in the following chapters.

5 The Solvent Relaxation Method

The solvent relaxation method (SRM) belongs to specific, fairly advanced variants of time-resolved fluorescence measurements. It has been used less in polymer science than fluorescence depolarization, quenching, or FRET, but it provides unique information on the polarity and microviscosity of the solvate shell of the probe (or more precisely on the mobility of molecules in the solvate shell) and interesting papers on the systems of low-molar-mass compound and also on self-assembled colloid and polymer systems have appeared in recognized journals in recent years [35–43]. Before discussing the use of SRM for the investigation of polymer systems, we will outline the principle of the method for a dilute solution of fluorophores in an isotropic polar solvent. We would like to point out that the probes used in SMR should be polarity dependent, i.e., they should exhibit a large shift in the emission band with polarity, but their photophysics should be simple (see the later discussion); otherwise interpretation of the data becomes complicated and specific for a given system—without the possibility of formulating general conclusions.

The principle of the solvent relaxation method is depicted in Fig. 5 for a fluorophore immersed in a polar solvent (with equilibrium ground-state relative

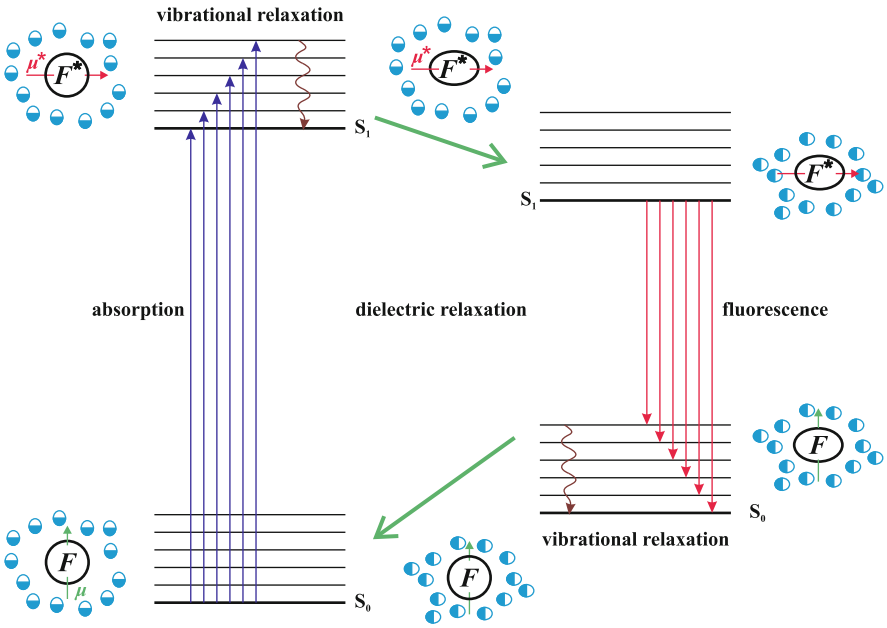

Fig. 5 Solvent relaxation: energies of the electronic states of a solvated fluorophore are depicted by *bold lines*, vibrational states by *thin lines*; the *long arrows* and *wavy lines* show individual processes; the changes of the dipole moment and geometry of the fluorophore upon excitation and emission are depicted by different orientations of the *short arrow* and the ellipsoidal prolongation. The changes in the arrangement and orientation of polar solvent molecules are indicated by *bicolor circles*. Adapted from Springer, Self Organized Nanostructures of Amphiphilic Block Copolymers I, 241, 2011, 187–249, figure 4, [2]. Copyright 2011. With kind permission from Springer Science and Business Media

permittivity, ε) and a higher dipole moment $\boldsymbol{\mu}_1$ in its excited state than that in the ground state $\boldsymbol{\mu}_0$. The vertical axis corresponds to the Gibbs free energy of the solvated fluorophore. As already mentioned, a necessary condition for the absorption, as well as for the emission of a photon, is a change in the dipole moment. Prior to excitation, the orientation of the polar solvent molecules in the solvation shell minimizes the Gibbs free energy, G, of the ground-state system. In this case, it is related mainly to the electrostatic interaction of the dipole moment of the fluorophore with the dipole moments of close solvent molecules. The fluorophore undergoes fairly rapid translational and rotational diffusion, but the solvent molecules are smaller than the fluorophore and the optimum structure of the solvate shell catches up with the random motion of the fluorophore and the time fluctuations in G are small.

As the absorption of a photon and a consequent redistribution of the "electron cloud" occur in less than 10^{-15} s, the change in the dipole moment, $\Delta\boldsymbol{\mu} = \boldsymbol{\mu}_1 - \boldsymbol{\mu}_0$, of the fluorophore (to be exact, the part corresponding to the redistribution of electrons) is almost instantaneous compared with the rate of motion of the nuclei and

the surrounding molecules. Therefore, immediately upon excitation, the geometry of the fluorophore (bond lengths and angles) and the arrangement of molecules in the solvate shell still correspond to the ground state. The solvation is not optimum and the Gibbs free energy soon after the excitation is higher than that of the properly equilibrated excited system. Two processes contribute to the minimization of G in the excited state: vibrational relaxation (which recovers the equilibrium geometry of the excited probe on a timescale of ca. 10^{-12} s) and slightly slower reorganization of the solvate shell (the rate of which depends on the solvent viscosity and temperature), which proceeds on a sub-nanosecond scale at ambient temperatures in nonviscous solvents). While the first process occurs in all the systems and causes the inherent Stokes red shift of the fluorescence with respect to the absorption regardless of the polarity of the probe and of the solvent, the second one takes place only in polar solvents and adds a polarity-dependent contribution to the Stokes shift. The extent of solvent relaxation depends on the strength of the dipole–dipole interactions between the fluorophore and molecules in the solvate shell (i.e., on the change in the dipole moment and on the local polarity of the microenvironment) and its rate depends on the mobility of the solvated molecules (i.e., on the local viscosity of the microenvironment). In nonviscous solvents, it proceeds quite rapidly and it can partially overlap with the vibrational relaxation. In this case, complete dielectric relaxation is usually complete before the emission of a photon (i.e., before the emission of an overwhelming majority of the photons in macroscopic samples), which means that most photons are emitted from the fully relaxed state S_1 on a nanosecond timescale. However, the emission is a stochastic process and its rate decays exponentially. Hence, at short times, some "hot photons" are emitted from non-relaxed states with higher energy than that of the fully relaxed state S_1 and ultrafast time-resolved measurements enable their detection.

Even though fluorescence decay in macroscopic systems proceeds in the nanosecond time region, the act of single emission (and transition from S_1 to S_0) occurs in times shorter than 10^{-15} s. Hence, immediately after the emission of a photon from the fully relaxed S_1 state, the geometry of the fluorophore and the structure of the solvate shell do not correspond to the ground state S_0, but still correspond to the excited state. This is followed by a cascade of processes that resemble the mirror image of the above-described relaxations after the excitation. However, it is necessary to bear in mind that the reorganization of the solvent shell at short times (after the "hot emission") requires less solvent reorganization because it proceeds from a non-equilibrated (high energy) S_1 state back to S_0 and the solvation shells of both states roughly correspond to the relaxed S_0 state.

A simple quantitative treatment of the solvent relaxation-induced Stokes shift is based on a model that assumes that the fluorophore is located in a cavity with radius a in a dipolar medium characterized by the bulk dielectric permittivity ε and refractive index n (we should recall that the high-frequency limit of the dielectric permittivity ε_∞ equals the square of the refractive index n^2). Classical treatment yields the Lippert equation [44] describing the difference, $\Delta\tilde{\nu} = \tilde{\nu}_A - \tilde{\nu}_F$, between the wavenumbers of the emission and absorption maxima of the fully relaxed system:

$$\Delta\tilde{\nu} \sim \frac{2(\mu_1 - \mu_0)^2}{hca^3}\left(\frac{\varepsilon - 1}{2\varepsilon + 1} - \frac{n^2 - 1}{2n^2 + 1}\right) \tag{11}$$

where h is the Planck constant and c is the speed of light in a vacuum, and $\mu_1 - \mu_0$ is the difference between magnitudes of corresponding dipole moments. This equation makes it possible to examine the local polarities of nano- to microdomains in heterogeneous systems (provided that the partitioning of the fluorophore between different domains can be estimated independently).

In this chapter, we generally avoid discussion of the technical details of time-resolved measurements, such as the principle of the time-correlated single photon counting technique, extraction of the net decay curve by the deconvolution method, etc. However, in this case, it is necessary to outline the principle of the solvent relaxation measurement and data evaluation (called "spectral reconstruction"). Application of the solvent relaxation method requires the measurement of a number of decay curves at different emission wavelengths, λ_{Em} (excited at the same excitation wavelength, λ_{Ex}). All the decay curves are measured with approximately the same statistics and are normalized. Emission from states populated immediately upon excitation yields decays in the blue part of the emission spectrum. The red-shifted decays correspond to emission from states which are not present at the very beginning and are created relatively slowly by the relaxation of the solvate shell on nanosecond and sub-nanosecond timescales. Therefore, the decay curves for longer wavelengths contain the rising (built-up) part at short times and later they achieve a maximum and finally decrease. The next step is reconstruction of the time-resolved spectra. It also requires measurement of the steady-state emission spectrum (excitation at the same wavelength as the time-resolved decays), because the intensity of the emission at λ_{Em} and t is proportional to the product of the steady-state intensity for a given wavelength, $F_{SS}(\lambda_{Em})$, and the fraction of the time-dependent intensities, $f(\lambda_{Em},t) = F_{TR}(\lambda_{Em},t)/F_{TR}(\lambda_{Em},t=0)$. The properly normalized intensities of the time-resolved spectra, $F_{TRS}(\lambda_{Em},t)$, are given by the relation

$$F_{TRS}(\lambda_{Em}, t) = \frac{F_{SS}(\lambda_{Em})F_{TR}(\lambda_{Em}, t)}{\int_0^\infty F_{TR}(\lambda_{Em}, t)dt} \tag{12}$$

and the final output is the normalized time dependence of the frequency of the emission, $\nu_{Em}(t)$ in the form of the correlation function (wavelengths of intensity maxima of emission bands are usually converted to the frequency scale):

$$\frac{[\nu_{Em}(t) - \nu_{Em}(t=\infty)]}{[\nu_{Em}(t=0) - \nu_{Em}(t=\infty)]} = C(t) \tag{13}$$

While the estimation of $\nu_{Em}(t=\infty)$ in the fully relaxed systems is not a problem, the value immediately upon excitation is often subject to ambiguities, especially in nonviscous highly polar solvents. In a number of cases, the relaxation is simply too

fast for the time resolution of the detection used and $v_{Em}(t=0)$ cannot be detected with sufficient accuracy. One more complication has to be taken into account in heterogeneous systems. Some amphiphilic or strongly nonpolar fluorophores, which bind to nanoparticles and are used in studies of nanoparticle solutions, are not sufficiently soluble in pure polar solvents and form self-quenched aggregates. Heterogeneous systems will be treated in the next part, but the estimation of $v_{Em}(t=0)$ is a general problem and therefore will be briefly discussed here. Maroncelli et al. [45] proposed an approximate method that can be used in all cases. It assumes knowledge of the frequencies of the absorption band of the probe in the polar solvent employed, $v_{A,p}$, and in a reference nonpolar solvent, $v_{A,np}$, which do not change with time and can be easily measured by UV–vis absorption spectroscopy providing that the probe is soluble in both solvents. Further, it requires knowledge of the emission frequency in a nonpolar solvent, $v_{Em,np}$, which again does not change with time, because the solvent relaxation proceeds only in polar solvents. Hence, it corresponds to the frequency of the maximum of the steady-state emission spectrum and can be estimated without problems. The value of the frequency in the polar solvent immediately upon excitation, $v_{Em,p}(t=0)$, can be evaluated from the simple formula

$$\nu_{Em,p}(t=0) = \nu_{Em,np} + (\nu_{A,p} - \nu_{A,np}). \tag{14}$$

6 Solvent Relaxation in Heterogeneous Systems

So far, a large number of low-molar-mass systems have been studied by ultrafast fluorescence techniques in sub-nanosecond time regions [35–39]. Recently, a relatively slow (nanosecond) relaxation process proceeding in mixed low-molar-mass solvents, consisting in redistribution of components of the solvent mixture in the solvate shell of the fluorophore upon the excitation, has also been reported [40–43, 46, 47]. However, an important part of experimental studies is still concerned with "relatively slowly relaxing" biological systems, such as lipid membranes [48–50], proteins [51, 52], nucleic acids [53], and also colloidal [54] and polymer systems [55–57].

In the next part, we will focus our attention on nanosecond processes that occur in shells of self-assembled polymer micelle-like nanoparticles in aqueous media [56, 57]. Fluorescent probes that strongly bind to the nanoparticles have usually been employed to obtain information on the shell or on the immediate vicinity of nanoparticles. Suitable probes include amphiphilic fluorophores, i.e., fluorescent surfactants, such as prodan, laurdan, or patman (see chapter "Fluorescence Studies of Polymer Containing Systems", Fig. 2). They contain a fairly polar fluorescent head-group and a nonpolar aliphatic tail, which secures the favorable "hydrophobic interaction" and sorption on polymer nanoparticles. They bind to micelles [55, 56] and their localization depends on the polarity of the head-group and on the length of the tail. In the case of patman, the strongly polar head is usually located in the peripheric part of the solvated shell and the nonpolar tail is oriented towards the

core/shell interface, i.e., buried in the inner shell. Probes with less polar heads (laurdan) can be buried quite deep in the nanoparticle (close to the core/shell interface). The micellar shell represents a fairly concentrated polymer system, which does not contain enough water in its innermost part (close to the core-shell interface) and the solvation of some components can be incomplete. The buried probe competes with polymer segments for water molecules and the complex solvent redistribution is significantly slowed down and differs in many aspects from the simple dielectric relaxation in isotropic low-molar-mass solutions.

The complexity of the dielectric response derives from the fact that micellar systems are "micro-heterogeneous" and contain components that differ significantly in size and in mobility: small and mobile solvent molecules, slightly larger fluorescent probes, and fairly large nanoparticles (with characteristic dimensions ranging from several nm up to 10^2 nm and molar masses 10^6–10^7 g/mol). The properties of nanoparticles that influence the fluorescence of probes, e.g., the density and effective polarity of the water-soluble shell, the degree of ionization in weak polyelectrolyte shells, solvation of shell-forming units, and water structure, vary in the direction from the central part of the nanoparticle to the periphery [58, 59]. Appreciable changes occur at distances comparable with the size of the fluorophore. Therefore, not only the redistribution of water molecules upon excitation but also the motion of the fluorophore with respect to the nanoparticle can occur during the lifetime of the excited state. In some systems, partial redistribution of amphiphilic probes between the core and shell has also been observed [55].

In micro-heterogeneous systems, the time dependence of the half-width of the time-resolved emission band should be measured and plotted as a function of time because it provides important information on the extent of the monitored process. It has been shown [60] that the half-width should be more or less constant in homogeneous systems (in fact, it should decrease slightly). The process proceeds differently in spatially inhomogeneous systems. Because the properties of the system vary in space, individual fluorophores distributed in different parts of the system are not equivalent and their solvent shells respond at different rates to the changing local electric field. This inhomogeneity gives rise to a new phenomenon that reflects the time distribution of the relaxation phases of different solvent shells. The observed transient inhomogeneity increases significantly at intermediate times and attenuates at long times [60].

Monitoring of the half-width of the emission band provides information about whether the entire process, or just a part of it, was included within the time window of the experiment. If only a decrease is observed, the early part of the relaxation process is beyond the time resolution of the relevant apparatus. In contrast, if only the rising part is observed, the process is slow and the fluorescence lifetime is too short and does not allow monitoring of the entire relaxation process. The following chapters give some examples of studies of self-assembling polymer systems by the solvent relaxation method.

7 Time-Resolved Fluorescence Anisotropy

As already explained, the probability of photon absorption by a given molecule depends on a number of factors (see the optical selection rules). If polarized light is employed [61], it also depends on the orientation of the absorption transition dipole moment, $\boldsymbol{\mu}_{\mathrm{A}}$, with respect to the polarization plane of the excitation light (described by the angle ϕ). Molecules with their absorption dipole moment parallel to the polarization plane of the excitation light are excited preferentially, while those oriented perpendicularly are not excited at all. For a general orientation with angle ϕ, the dipole moment can be decomposed into parallel and perpendicular components, $\boldsymbol{\mu}_{\mathrm{A}}\cos\phi$, and $\boldsymbol{\mu}_{\mathrm{A}}\sin\phi$, respectively, and the excitation probability is proportional to $(\cos\phi)^2$.

Fluorophores in solutions (i.e., their dipole moments) are oriented randomly prior to excitation and undergo rotational diffusion. Nevertheless, immediately upon excitation by a sufficiently intense ultrafast polarized light pulse, the population of excited molecules with absorption dipole moment parallel to the plane of the polarized excitation light predominates. Several processes contribute to the relaxation of the anisotropic population of excited molecules; in addition to processes that deplete the excited state (both radiative and nonradiative): (1) the rotational Brownian motion of fluorophores and (2) the excitation energy migration among fluorophores also play an important role. The probability of nonradiative energy migration depends strongly on the distance between the fluorophores (see the part describing energy transfer). Consequently, the rate of the latter depolarizing process in macroscopic solutions can be significantly suppressed at high dilutions. The absorption and emission transition dipole moments, $\boldsymbol{\mu}_{\mathrm{A}}$ and $\boldsymbol{\mu}_{\mathrm{E}}$, can form any angle ω , but they are usually parallel in fluorophores that contain symmetry planes, which means that the emission at early times following polarized excitation is also strongly polarized in the same plane and the time-dependent fluorescence anisotropy provides information on the depolarization processes; in dilute systems, it corresponds predominantly to the rotational diffusion of the probe. Relaxation of the system can be followed by measuring the time-resolved anisotropy,

$$r(t) = \frac{\left[I_{\parallel}(t) - I_{\perp}(t)\right]}{\left[I_{\parallel}(t) + 2I_{\perp}(t)\right]} \tag{15}$$

where $I_{\parallel}(t)$ and $I_{\perp}(t)$ are the parallelly and perpendicularly polarized emission intensities at time t after the excitation, respectively. The sum $S(t) = \left[I_{\parallel}(t) + 2I_{\perp}(t)\right]$ in the denominator is proportional to the population of molecules in the excited state, i.e., it represents the total fluorescence intensity and does not depend on the orientation of the molecule. The polarized fluorescence decay $I(t,\phi)$ measured at arbitrary angle ϕ can be expressed in the following form:

$$I(t,\phi) = \frac{1}{3}\left[1 + \left(3\cos^2\phi - 1\right)r(t)\right]S(t) \tag{16}$$

In measurements at the so-called "magic angle," i.e., with the detector of polarized light oriented at $\phi_M = 54.7^\circ$ with respect to the polarization plane of the excitation beam, the experiment directly yields the decay $I(t,\phi_M) = S(t)$ unaffected by anisotropy, because in this case: $(3\cos^2\phi_M - 1 = 0)$.

From a theoretical point of view, the experimentally accessible time-resolved anisotropy, $r(t)$, represents the autocorrelation function of orientations of the emission transition dipole moment $\boldsymbol{\mu}_E(t)$ at time t and the absorption transition dipole moment $\boldsymbol{\mu}_A(t=0)$ at the instant of excitation, $t = 0$, and can be expressed as

$$r(t) = 2/5\langle P_2(\boldsymbol{\mu}_A(t=0)\boldsymbol{\mu}_E(t))\rangle \tag{17}$$

where P_2 is the second-order Legendre polynomial and the brackets denote the ensemble averaging. The initial anisotropy is given by $r(t=0) = (0.6\cos^2\omega - 0.2)$ and depends on the mutual orientation of $\boldsymbol{\mu}_A(t=0)$ and $\boldsymbol{\mu}_E(t=0)$. The two following limiting values are acquired for parallel (the highest positive value 0.4) and perpendicular (the lowest negative value -0.2) orientation. Even though perpendicular orientation of both dipole moments is not very common, such situation can occur if the fluorophore is excited to a higher state than the emitting state and the molecule (e.g., perylene, [12]) undergoes one or more nonradiative transitions between different excited states with mutually perpendicular orientation of dipole moments before emission. For completeness, it should be pointed out that the emission is totally depolarized from the very beginning in molecules in which the angle between dipole moments corresponds to the magic angle. On the other hand, in perfectly ordered systems of fluorophores with mutually parallel absorption and emission dipole moments, e.g., in a fluorophore crystal with corresponding dipole moments that are mutually parallel, the anisotropy defined by Eq. (15) would theoretically be $r(t) = 1$ and would not depend on time. In real crystals, $r(t)$ can be slightly lower due to defects in lattice structure and vibrations.

In a number of fluid systems, rotational diffusion proceeds on timescales comparable with the fluorescence decay and can be employed to study the viscosity of the microenvironment, segmental motion of the polymer chains, local geometrical constraints, and changes in the above characteristics caused by external stimuli, etc. In nonviscous systems of small molecules, fluorescence anisotropy due to rotational diffusion usually decays faster than fluorescence, but in viscous solutions and also in various polymer and biopolymer systems, full angular randomization is often achieved at times much longer than that corresponding to the depletion of the excited state and it is not possible to monitor the whole fluorescence anisotropy decay experimentally. However, careful data fitting (based on an appropriate model) provides reasonably accurate time characteristics together with the so-called "residual anisotropy" value (see the later discussion for its physical meaning).

8 Models of Rotational Diffusion (RD) and Their Advanced Variants

In dilute systems of small molecules (where energy migration can be neglected), the anisotropy decays are commonly fitted to curves derived on the basis of the rotational diffusion model. There exist several variants of this model. The oldest and simplest approach, which has mostly been used for interpretation of the data obtained from systems of small molecules, is known as the Debye hydrodynamic model [62–69]. The fluorophore is modeled by a solid (generally asymmetrical) ellipsoid immersed in a viscous liquid. Its rotational diffusion coefficient is given by the Stokes–Einstein equation [70] and its orientation with respect to the fixed laboratory system of coordinates can be characterized by three Euler angles $\boldsymbol{\Omega}$. It is assumed that the molecule rotates through a very small angle between individual collisions and its reorientation can be described by the rotational diffusion equation:

$$\frac{\partial}{\partial t} f(\boldsymbol{\Omega}, t) = -f(\boldsymbol{\Omega}, t), \tag{18}$$

which yields the probability density $f(\boldsymbol{\Omega}, t)$ describing the orientation of the molecule at time t (expressed by Euler angles $\boldsymbol{\Omega}$) regardless of the electronic state. $\mathbf{H}$ is the Hamiltonian operator, $\mathbf{H} = \sum_{i=1}^{3} \sum_{j=1}^{3} \mathbf{L}_i D_{ij} \mathbf{L}_j$, $\mathbf{L}_i$ is the quantum mechanical operator of the angular momentum defined according to Rose [71], and D_{ij} are the components of the diffusion tensor. Knowledge of $f(\boldsymbol{\Omega}, t)$ allows calculation of the polarized intensities $I_{\parallel}(t)$ and $I_{\perp}(t)$ and consequently the time-resolved anisotropy, $r(t)$, as the sum of several terms, each of them decaying exponentially with time [72]:

$$r(t) = \sum_{i=1}^{5} A_i \exp\left(\frac{-t}{\tau_{ri}}\right) \tag{19}$$

where the individual correlation times τ_{ri} are functions of the principal components of the diffusion tensor, i.e., $\tau_{ri} = f(D_1, D_2, D_3)$ and the pre-exponential factors depend both on the components of the diffusion tensor and on the orientation of the absorption and emission transition dipole moments, $\boldsymbol{\mu}_A$ and $\boldsymbol{\mu}_E$, respectively (angles α_j and β_j), with respect to the principal axes of diffusion, i.e., $A_i = f(D_1, D_2, D_3, \alpha_j, \beta_j)$. In the general case of a low symmetry molecule, there are five exponential terms, but only three correlation times τ_{ri} are independent. If the symmetry of the fluorophore increases, the number of exponentials decreases. As it is difficult to discern more than two exponential terms experimentally (the nominator in Eq. (15) is a fairly small difference between two large numbers, while the denominator is their sum), only the cases when the number of exponentials reduces to one or two are important in practice. This can happen [73], e.g., if the fluorophore can be approximated by a rotationally symmetric ellipsoid $D_1 = D_{\parallel} \neq D_2 = D_3 = D_{\perp}$ (symmetric-top) and $\boldsymbol{\mu}_A$ or $\boldsymbol{\mu}_E$ are simultaneously perpendicular to the axis of

rotational symmetry, the anisotropy decay is described by two exponential terms (two correlation times). Other possibility for two rotational correlation times is that $\boldsymbol{\mu}_A$ or $\boldsymbol{\mu}_E$ is parallel with one of diffusion axes. If $\boldsymbol{\mu}_A$ and $\boldsymbol{\mu}_E$ are parallel for symmetric top, single exponential decay occurs (one correlation time). Single exponential decay is also obtained for a spherical top, i.e., if all the main components of the diffusion tensor are equal, $D_1 = D_2 = D_3$.

Because the fluorophore interacts with solvent molecules and binds them, creating the solvate shell, the D_i values cannot be predicted on the basis of a simple atomistic model of the rotating molecule. The solvation depends both on the fluorophore and on the solvent and varies considerably from one system to another [74]. Two limiting situations have been considered in the literature: (1) the stick condition—when the first solvent shell moves together with the fluorophore, and (2) the slip condition, i.e., the opposite extreme situation, when the solvent molecules do not bind to the fluorophore. However, the rotation of the fluorophore is still not free in the latter case. It is hindered by the necessity of redistributing the molecules of the solvent to create the free space necessary for a change of the fluorophore position, which generates the hydrodynamic friction. Redistribution of the solvent molecules depends strongly on the shape of the rotating object. This is quite small for spherical particles. The rotation of a prolate ellipsoid around its long axis does not require almost any solvent redistribution, but that around the short axes (perpendicular to the long one) does require redistribution and the corresponding D_i value obtained by fluorescence measurement is significantly larger than the net value based on the atomistic model. The stick condition assumes that, in addition to the motion of the firmly bound solvent shell, a non-negligible displacement of solvent molecules occurs at longer distances from the fluorophore for the same reasons as discussed above.

Very interesting special anisotropy decay has been predicted for a symmetric molecule approximated by disc with perpendicular orientation of $\boldsymbol{\mu}_A$ and $\boldsymbol{\mu}_E$, both lying in the plane of the disc, which we designate, for a clear and unambiguous discussion, as the *yz* plane and assume that the light beam comes in the *x* direction and polarization plane is *xz* (see Fig. 6a). The net principal D_i components of the molecule in the direction of the main symmetry axes C_∞ (axis *x*) and in the directions of the two perpendicular axes C_2 in the disc plane (the *z* and *y* directions coinciding with the orientations of $\boldsymbol{\mu}_A$ or $\boldsymbol{\mu}_E$, respectively) do not differ much. However, the rotation of the disc around the *x* axes does not require almost any redistribution of the solvent molecules, while the rotations around *y* or *z* require the continuous displacement of a number of solvent molecules and the corresponding correlation time τ_{r2} is ca. 10 times longer than τ_{r1}. Because $\boldsymbol{\mu}_A$ and $\boldsymbol{\mu}_E$ are perpendicular to each other, $r_0(t = 0) = -0.2$. The anisotropy increases rapidly at short times after excitation (with τ_{r1}) as a result of rapid 1D rotational diffusion around the *x* axis, which randomizes the orientations of the excited molecules in the *yz* plane (in which both dipole moments lie) and eliminates the excess of excited molecules emitting perpendicularly polarized light with respect to the excitation polarization. Note that full randomization of the orientations of the excited fluorophores in 3D is not achieved at short times because the rotations around the second and third axis are slow. This is why $r(t)$ does not converge to

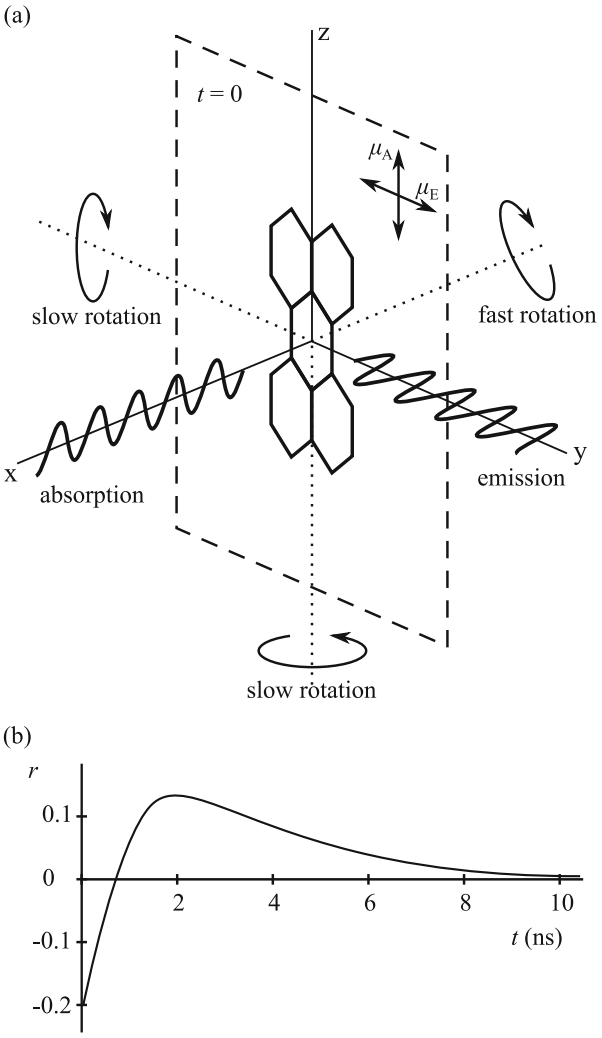

Fig. 6 Unusual shape of the fluorescence anisotropy decay curve, obtained, e.g., for perylene excited to the S_2 state, i.e., in the UV region far from the "zero–zero" transition. (**a**) Schematics explaining physical reasons of the non-monotonous time dependence, which is due to a combination of two facts: (1) the absorption and emission dipole moments are perpendicular to each other, and (2) hydrodynamic friction affects the rotation of the molecule with respect to different axes of symmetry. (**b**) Schematic shape of experimental curve, $r(t)$. Timescale depends on the viscosity of the solvent used

zero, but increases to slightly positive values 0.1–0.2 (depending on the difference between the effective D_i values) and then slowly decays to zero (with τ_{r2}) as the 3D randomization continues. The example described above is not only interesting from the theoretical point of view, but it is also important in practice, because it has been experimentally observed for commonly used fluorophores, such as perylene. If perylene is excited in the short wavelength part of its absorption spectrum to the S_2 state, which is polarized perpendicularly to the S_1 state, the nonradiative transition $S_2 \rightarrow S_1$ takes place first and then the perpendicularly polarized emission (with respect to the absorption) occurs [75, 76]. Schematic shape of the anisotropy curve corresponding to the above-described behavior of perylene and analogously behaving planar fluorophores is shown in Fig. 6b. In experiments, only two

(maximally three) rotational correlation times can be evaluated with reasonable accuracy. The experimental accuracy depends mainly on the difference between the individual correlation times and on the ratio of the rate of the orientation relaxation to the fluorescence decay. This means that both the experimental pre-exponential factors A_i and correlations times τ_{ri} frequently represent the effective weighted averages of parameters corresponding to several different rotations. The best resolution is usually obtained for systems where the anisotropy decays are slightly faster than the fluorescence intensity decays. Moreover, the fact that mutual orientation of $\boldsymbol{\mu}_A$ and $\boldsymbol{\mu}_E$ is not known for a number of fluorophores hinders interpretation of the anisotropy data. Theoretical analysis predicts that experimental coefficients A_i may depend on the excitation and emission wavelength, but should not depend on the viscosity of the medium and on the temperature: as has already been explained, the initial anisotropy $r_0(t=0)$ for perylene excited to S_2 is -0.2, while $r_0(t=0)$ is close to 0.4 for S_1 excitation. In isotropic systems of small mobile molecules, the anisotropy should decay to zero at long times and therefore the residual anisotropy should also be zero, $r_\infty = 0$. A nonzero value r_∞ means that the rotational movement in 3D is restricted due (1) to bonding (or incorporation) of the probe (in)to a very large and heavy rigid object or (2) to strong anisotropy of the medium. In the first case, some correlation times are extremely long compared with the fluorescence lifetime and the true r_∞ value cannot be obtained experimentally; in the second case, the rotation does not proceed freely in all 3 dimensions.

The rotational diffusion model has been revised and improved by several authors and a few advanced models that remove the most severe simplifications have been proposed. The extended diffusion model (ED) eliminates the condition of small angular changes between individual collisions [77–81], i.e., it assumes that reorientation of the molecules proceeds in a sequence of mutually independent (both short and long) diffusion steps. Molecules rotate freely and the angular momentum does not change between the collisions. The probability of steps of different length is given by the Poisson distribution. Collisions between molecules are considered to be fast events compared to the average time of the diffusion steps between them. Two variants of the ED model, differing in the character of the angular momentum changes, have been proposed. The so-called J-diffusion assumes that changes in the orientation of the angular momentum are completely random (i.e., all changes in the direction of rotation are equally probable), but changes in its magnitude obey the Boltzmann distribution. The M-diffusion variant assumes that the angular momentum magnitude does not change after the collision; only its orientation changes randomly.

In both cases, the time-resolved anisotropy decay acquires a complex form of an infinite series. Gordon [77] has shown that the decay may, in special cases, exhibit damped oscillations, which has been observed experimentally, but the original RD model was unable to offer an explanation of this rather exotic behavior. Numerical calculations by McClung [79] validated the ED prediction for spherical molecules. For asymmetric molecules, the calculations confirmed the formulae based on the J-diffusion model and indicated that the assumptions used in the M-diffusion model are less realistic [81].

Another attempt to improve the RD model was made by Fixman and Rider for linear molecules in 1969 [82] and later by McClung for spherical and asymmetric top in the early 1980s [83, 84]. In accordance with the theoretical background employed (already existing in other fields of physics), the model is called the Fokker–Planck–Langevin (FPL) model. Theoretical treatment assumes that the rotational movement of a rigid molecule (e.g., ellipsoid) immersed in a viscous liquid is affected (1) by the slowly changing frictional force (depending on the viscosity of the solvent and fluorophore–solvent interactions) and (2) by fairly rapidly changing Brownian forces, which mimics collisions with solvent molecules. The model allows formulation and solution of the rotational Fokker–Planck equation for the conditional probability density that the molecule rotates at time t in a given direction with a particular angular velocity. The anisotropy decay is then expressed as a rapidly converging infinite series of exponentials. From the practical point of view, it is important that a strongly truncated series with only a few terms provides quite accurate values of the rotation correlation times of test systems. The FPL and ED models represent two very different approaches for treatment of the interaction of the fluorophore with the solvent molecules and for explaining the influence of the microenvironment on the rotation of the fluorophore. Both models eliminate the assumption of small diffusion steps, but the physical assumptions are quite different from each other. In the ED model, the molecules may undergo large changes in their orientation and in the magnitude of their angular momenta during collisions, which are considered to be almost instantaneous events compared with the length of the unaffected rotation between them. The FPL model employs the slowly changing friction force and more rapidly changing Brownian force. Its main difference with respect to ED is as follows: Because the two forces are balanced (to maintain a constant temperature of the system), a relatively large number of emulated collisions are required to cause a large change in the rotation of the fluorophore. Lévi et al. published a comparison of anisotropy decays based on ED and FPL with experimental data for linear and spherical molecules [85]. Both models offer an almost indistinguishable macroscopic description of the rotational motion of molecules in liquid media and it was not possible to decide which description is physically more relevant. The authors recommend great care and precaution when drawing conclusions from model fitting of experimental data.

Other interesting extensions of the RD model (similar to ED) include the partially relaxed rotation model (PRR) [86] for a symmetric-top rotor and its generalization, the 2τ model. The basic assumptions are based on the experimentally verified fact that the rotation of an oblong ellipsoid around its long symmetry axis C_∞ does not require almost any displacement of the surrounding molecules and is effectively free, but the tumbling motion accompanied by changes in the spatial orientation of this axis is a complex relaxation process controlled by collisions with solvent molecules. Hence the uncorrelated binary collisions affect only the motion in directions perpendicular to C_∞. Distribution of the angular velocities around C_∞ is given by the Maxwell–Boltzmann distribution and the relaxation of the tumbling motion is described by the characteristic time, τ_1. In a more general 2τ model, the relaxation of the rotation around C_∞ (described by τ_2) is

also considered. At the limit of long relaxation times, this model converges into (a) PRR, if $\tau_2 \to \infty$, (b) ED-J, if $\tau_1 \to \infty$, or (c) a free rotor (symmetric-top RD with slippery condition), if both $\tau_1 \to \infty$ and $\tau_2 \to \infty$.

9 Fluorescence Anisotropy in a System of Flexible Fluorescent Molecules

The time-resolved fluorescence anisotropy is a suitable tool for studying complex motion of polymer chains. However, the data must be interpreted with care and precaution. Fluorescence spectroscopy in general (and anisotropy in particular) provides indirect information on the studied host system. The more advanced is the experimental technique and the model used for fitting the data, the greater is the risk of misinterpretation. In fact, the basic assumption that the motion of the probe is a good indicator of that of the host system is the most problematic aspect. The rotation of dispersed probes is undoubtedly affected by the host system, but interpretation of the anisotropy results is difficult and often ambiguous. Moreover, only a few polymer and biopolymer systems (e.g., tryptophan-containing proteins, polyvinylcarbazole) are intrinsically fluorescent. In most other cases, the fluorophore has to be added to the host system. It can be simply dispersed in the solution and, in this case, it is usually called a "probe," or it can be chemically attached to the system of interest and then it is usually called a "label." Hydrophobic probes interact with hydrophobic domains formed within the polymer chain in aqueous or highly polar media and bind to them and therefore can be used for monitoring the behavior of specific parts of the chain, but the chemical attachment of a label (as a co-monomer within the chain or as a pendant group) provides a much better opportunity for detailed studies. However, one should bear in mind that the presence of the fluorophore in the chain (generally in the studied host system) always influences the properties of a tiny part of the chain/system. In spite of the fact that chemical modification is negligible and has almost no impact on the macroscopic behavior of the system, the fluorescence monitors the behavior of the small domain of the host system that has been affected. For safe interpretation of the fluorescence data for a polymer system, the fluorescence study should be combined with other methods that provide independent data, or it should be corroborated by already existing knowledge of the system. Only in these cases can the high potential of fluorescence methods be fully exploited.

An ideal fluorescence probe or label for anisotropy measurements should meet the following requirements:

1. It should specifically monitor the behavior of a known part of the molecule,
2. It should perturb the behavior of the host system as little as possible,
3. It should have simple spectroscopic properties (single exponential decay and a lifetime somewhat longer than the monitored anisotropy decay, etc.),

4. Its simple rigid shape and orientation of dipole moments should enable unambiguous interpretation of the anisotropy decay of the free probe in isotropic media,
5. Chemical attachment of the label to the polymer should enable simple interpretation of the fast components of anisotropy relaxation.

Because of the variability of fluorescent or fluorescently labeled polymers and the complexity of the relaxation processes that come into account, no general model for anisotropy decay in polymer systems has been proposed so far; however, a number of papers analyzing decays in different systems have been published [2, 87–96] and will be outlined in the next part.

If the fluorophore is part of a large flexible molecule, e.g., it is a co-monomer incorporated in a flexible polymer chain or a pendant group covalently attached to a polymer chain or to a large polymeric nanoparticle, its reorientation relaxation is a complex process, which includes (1) fairly slow rotation of the whole nano-object, (2) reorientation motion of the probe with respect to some specific parts of the chain or of the nanoparticle (e.g., with respect to nano-structured domains differing in flexibility or in other important properties), and (3) fairly fast motion of the polymer structural units and rotation of the fluorophore around one or more single bonds, if it is attached to the chain or to the nano-object by a linker. From the practical point of view, it is convenient to classify the molecules according to the ratio of the fast correlation time to the longest time, which describes the motion of the whole particle.

If the relaxation times are fairly fast and comparable, all of them can, in principle, be measured. Moreover, if such a particle is immersed in an isotropic medium, the fluorescence anisotropy decays to zero. For a number of high-molar-mass macromolecules and self-assembled polymer nanoparticles, the longest relaxation time is significantly longer than the fluorescence lifetime and exceeds the capabilities of fluorescence measurements because the excited state is depleted long before full 3D relaxation occurs, which means that, at times when the fluorescence intensity is low and converges to zero, the anisotropy is still high and poor statistics of the emitted photons does not allow reliable extrapolation and evaluation of the long relaxation time. In a relatively narrow nanosecond time window, the slow relaxation (often several order of magnitudes slower than the fast one) does not show any appreciable decrease in $r(t)$ and it seems that the anisotropy has already leveled-off in spite of the fact that the fluorescent macromolecule or nanoparticle is immersed in an isotropic medium. Therefore, the formulas used for fitting the data for a polymer system usually contain a constant term—the residual anisotropy, r_∞ (pre-exponential factor of the term corresponding to $\tau_{\text{slow}} \to \infty$).

The motion of fluorophores incorporated in the form of co-monomers in flexible chains has been studied by Monnerie, Valeur et al. in a number of papers [97–99] from the 1970s. Since the flexible chains usually contain atoms in the sp^3 hybridization of bond-forming orbitals, the authors assumed that the internal rotation of small parts of the chains mimics the rotation of the crankshaft, i.e., it represents a

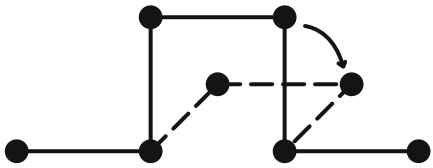

Fig. 7 Schematic representation of the crankshaft motion of the part of the polymer chain

simultaneous rotation of the part of the chain containing three segments connected by two external bonds to the rest of the chain (see Fig. 7).

Because the configurations of the chains which predominantly contain the "trans" and "gauche" conformations of short parts formed by four C atoms (in sp^3 hybridization) fit fairly well to the tetrahedral lattice (see chapter "Conformational and Dynamic Behavior of Polymer and Polyelectrolyte Chains in Dilute Solutions," Fig. 3), to a first approximation they assumed that the basic motion of the fluorophore can be described as a "jump-like rotation" on the tetrahedral lattice with one characteristic time, ρ (which depends on the characteristic "jump" frequency and the conformation structure of the chain), in the form [100, 101]:

$$r(t) = r_0 \exp\left(\frac{t}{\varrho}\right) \operatorname{erfc}\left(\sqrt{\frac{t}{\varrho}}\right) \tag{20}$$

In a more realistic model, which takes into account the fact that the chain conformation can deviate from the strict tetrahedral geometry, the anisotropy $r(t)$ acquires a more complex form (it contains two characteristic correlation times) [98]

$$r(t) = r_0 \exp\left(-\frac{t}{\theta}\right) \exp\left(\frac{t}{\varrho}\right) \operatorname{erfc}\left(\sqrt{\frac{t}{\varrho}}\right) \tag{21}$$

where θ is an additional correction relaxation time, which accounts for the perturbation relaxation of segments from orientations determined by the lattice. The derived equation has been used for the interpretation of experimental data on a solution of anthracene-labeled polystyrene in a good solvent (emission transition dipole moment parallel to the local part of the chain) and for 9,10-diphenylanthracene-labeled polystyrene (dipole moment perpendicular) [102–104]. The agreement was found to be satisfactory except for the short time region. Later, the crankshaft motion model was revised and the simultaneous rotation of several bonds was considered (not only two, but also three and nine simultaneously rotating bonds). Note that the original concept assumes the rotation of a part of the chain that contains three segments, but true rotation occurs only around two external bonds. The most important conclusion drawn from this model is the fact that the effective potential of hindered rotation is much lower if several bonds are involved compared with that for simple crankshaft motion.

Two models have been developed independently by Hall and Helfand [105] and by Monnerie at al. [106]. For the Hall–Helfand model (HH), the anisotropy decays according to the equation

$$r(t) = r(t=0)\exp\left(-\frac{t}{\tau_1}\right)\exp\left(-\frac{t}{\tau_2}\right)I_0\left(\frac{t}{\tau_1}\right) \tag{22}$$

and, in the second case known as the generalized diffusion and loss model (GDL), according to the equation

$$r(t) = r(t=0)\exp\left(-\frac{t}{\tau_1}\right)\exp\left(-\frac{t}{\tau_2}\right)\left[I_0\left(\frac{t}{\tau_1}\right) + I_1\left(\frac{t}{\tau_1}\right)\right] \tag{23}$$

where τ_1 and τ_2 are two correlation times and $I_i(t/\tau_1)$ are the modified Bessel functions. The mean correlation time τ_C can be calculated in the former case as

$$\tau_C = \left(\frac{1}{\tau_1\tau_2} + \frac{1}{\tau_2^2}\right)^{-1/2} \tag{24}$$

and in the latter case as

$$\tau_C = \left(\frac{2}{\tau_1\tau_2} + \frac{1}{\tau_2^2}\right)^{-1/2}\left[\frac{1}{\tau_1}\left\{\frac{1}{\tau_1} + \frac{1}{\tau_2} + \left(\frac{2}{\tau_1\tau_2} + \frac{1}{\tau_2^2}\right)^{1/2}\right\}^{-1} + 1\right] \tag{25}$$

Ediger et al. synthesized anthracene-labeled polystyrene and very carefully measured the anisotropy decays in a number of solvents of differing viscosity. They obtained very good data and used both models for analyzing anisotropy decays. Nevertheless, the experimental papers published by Ediger et al. are somewhat confusing. In their first paper [103], they concluded that the GDL model provides slightly better fits than the HH model, but 1 year later, in their second paper [104], they announced that the HH model is actually better than the EDL model. In fact, the differences were negligible and the two models provided fits of comparable quality. The Hall–Helfand model suffices with simpler mathematical treatment, which is more attractive for experimentalists, but both models involve two fitting parameters and, at the present time with advanced computers (in contrast to the epoch 20 years ago), complicated mathematical formulas for data treatment do not cause any problems.

Because the fluorophores are often attached by a single bond or by a short linker to a fairly large (roughly spherical) rigid macromolecule or nano-object, a model of a fluorophore rotating around one axis attached to a large spherical object was described by Gottlieb and Wahl [107]. The axis of rotation is assumed to be fixed in a radial position with respect to the bulky rigid macromolecular object (e.g., globular protein) and the fluorophore can either (1) freely rotate without any

hindrance (free internal rotation) or (2) perform a temperature-activated jump diffusion among discrete positions (T-JD). The following expression for $r(t)$ has been obtained for the free internal rotation:

$$r(t) = \exp\left(\frac{-t}{\tau_{cM}}\right)\left[\alpha_1 + \alpha_2 \exp\left(\frac{-t}{\tau_{cF}}\right) + \alpha_3 \exp\left(\frac{-2t}{\tau_{cF}}\right)\right] \tag{26}$$

where τ_{cM} and τ_{cF} are the depolarization correlation times of the particle and the fluorophore, respectively, which can be interpreted in both cases as the neat rotation correlation times, and α_i are constants depending on the orientation of transition dipole moments with respect to the axis of rotation of the fluorophore. The time-resolved anisotropy $r(t)$ has a similar form for the T-JD model:

$$r(t) = \exp\left(\frac{-t}{\tau_{cM}}\right)[\alpha_1 + \alpha_2 \exp(-Kwt)], \tag{27}$$

but the parameters have different physical meanings; K is the normalization constant, w is the jump frequency, and α_i depends on the angles between the transition dipole moments and the axis connecting the fluorophore with the bulk globule. A more general model for a freely rotating fluorophore attached to a more slowly rotating nonfluorescent symmetrical carrier was described by Burghardt [108] and a similar system with more complex relaxation processes was studied by Tanaka et al. [109] (internal rotation under the potential barrier). Numerical simulations based on this model were able to fit experimental decays from tryptophan in cytochrome C very well [110]. A discontinuous jump model for large carriers with fluorophores that can acquire a finite number of positions has also been published by Weber [111].

Szabo proposed an interesting model-free formula for the time-resolved anisotropy in a macroscopically isotropic system [112]. He expressed $r(t)$ as the autocorrelation function of orientations of the emission dipole moment at time t and absorption dipole moment at time $t = 0$ in a form suitable for general treatment of various systems, and particularly those with possible internal rotation:

$$r(t) = \frac{2}{5} \frac{\left\langle\left\langle k_F(t)\rho(v,t)P_2\left(\boldsymbol{\mu}_E(t)\cdot\boldsymbol{\mu}_A(t=0)\right)\right\rangle\right\rangle}{\left\langle\left\langle k_F(t)\rho(v,t)\right\rangle\right\rangle} \tag{28}$$

The physical meaning of the individual symbols is as follows: $k_F(t)$ is the time-dependent rate constant of the radiative depletion of the excited state, $\rho(v,t)$ is the normalized time-dependent emission spectrum, i.e., the denominator $\langle\langle k_F(t)\rho(v,t)\rangle\rangle$ describes the total fluorescence, $S(t)$, P_2 is the Legendre polynomial of the second order which correlates with the mutual angular orientations of $\boldsymbol{\mu}_E(t)$ and $\boldsymbol{\mu}_A(t=0)$, and denotes averaging with respect to possible orientations and energy states. He also employed the master equation, which describes the time change of the conditional probability $p\left(i,\boldsymbol{\Omega};t/(j,\boldsymbol{\Omega_0};t=0\right)$ that the fluorophore is in energy state i and

its orientation is described by three Euler angles $\boldsymbol{\Omega}$ at time t, if it was in electronic state j and its orientation was $\boldsymbol{\Omega_0}$ at $t = 0$. This equation has the form

$$\frac{\partial}{\partial t}\left[p\left(i, \boldsymbol{\Omega}; t/(j, \boldsymbol{\Omega}_0; t = 0)\right]\right. = \{\boldsymbol{L}(i, \boldsymbol{\Omega}) - \boldsymbol{k}(i, \boldsymbol{\Omega})\} p\left(i, \boldsymbol{\Omega}; t/(j, \boldsymbol{\Omega}_0; t = 0), \quad (29)\right.$$

where $\boldsymbol{L}$ is the operator, which, in addition to the changes in the angular momentum, also comprises the electronic transitions and $\boldsymbol{k}(i,\boldsymbol{\Omega})$ is the complex rate constant of irreversible transitions. The explicit form of the operator $\{\boldsymbol{L}(i, \boldsymbol{\Omega}) - \boldsymbol{k}(i, \boldsymbol{\Omega})\}$ results from the particular model used for describing the system of interest. The set of integro-differential Eq. (29) makes it possible to consider and include a number of phenomena in a unified fashion. It can account for energy migration and transfer, because the rate constants $\boldsymbol{k}(i,\boldsymbol{\Omega})$ depend on the distance and mutual orientation of the fluorophores (and quenchers). Very general formulation of the problem permits treatment of the effect of heterogeneity of the medium and its effect on the emission characteristics. The analytical solution is possible only for a small number of particular forms of the $\boldsymbol{L}(i, \boldsymbol{\Omega})$ operator. Solution of the equation is generally feasible if the energy and orientation relaxations are uncoupled and also if the overall and internal relaxations are uncoupled.

Realistic description of the relaxation behavior of systems with possible internal rotation is very complex and almost all the models had to introduce simplifying (sometimes even oversimplifying) assumptions. In spite of a number of theoretical studies, interpretation of the experimental data is mostly highly intuitive and is based on semiempirical formulas.

10 Rigid Molecules in Anisotropic Medium

Fluorescence anisotropy studies are very common in biochemical and biological research. They have been widely used in the past two decades to study the structures of various biological membranes formed by lipid bilayers [113–117]. Hence, a number of appropriate models have been proposed for interpretation of the experimental data for membranes and other organized biopolymer systems. In spite of the fact that this review is aimed at synthetic polymers and does not concern biopolymers and biologically important systems, the motion of probes embedded in dense 2D polymer brushes and in dense inner parts of coronas of self-organized polymeric nanoparticles is similar to that studied in biological membranes and therefore it will be mentioned.

The movement of a fluorophore embedded in a bilayer (generally in an anisotropic medium) is controlled by the 3D potential preferring certain (nonequivalent) orientations of the fluorophore in all three dimensions. At long times upon excitation, the system does not relax completely in all 3D and the residual anisotropy is not zero. To date no general theory has been formulated; however, particular models for the most frequently studied systems have been published by a number

of researchers. In the following text, we will briefly outline the most important models developed for analyzing fluorescence anisotropy decays in membranes.

In most cases, the theories focus on symmetric-top fluorophores. Kinosita et al. [115] published one of the oldest suitable models. Its analysis is applicable for a macroscopically isotropic suspension of planar lipid bilayers, which are assumed to be large and immobile during the anisotropy decay measurement. Individual bilayer planes are oriented randomly with respect to the polarization plane of the excitation light (i.e., the fluorophores are also oriented randomly and uniformly in 3D), which means that the probability of excitation of probes in different bilayer planes mutually differs and the emission polarization is also strongly polarized at early times following excitation. Note that the angularly random orientation of small mobile fluorophores in an isotropic medium prior to excitation also yields polarized emission at early times following a short excitation pulse. It is important to realize that random orientations of individual bilayer planes, which yield the static isotropic properties of the suspension, do not average the time-resolved fluorescence response in all three dimensions. The motion of probes in bilayers is locally anisotropic and does not completely relax in 3D, because the positions of the bilayers are kinetically frozen during the lifetime of the excited state. The basic assumptions of the model can be summarized as follows: (1) the bilayer does not move at times relevant for the decay measurement, (2) the probe rotates around one axis, which can move, and its orientation undergoes the diffusion motion in the potential field, which is symmetrical with respect to the direction perpendicular to the bilayer plane and depends on the angle φ between the instantaneous orientation of the axis of rotation and its time-averaged (perpendicular) orientation. Due to the orientation constraint, the anisotropy does not decay to zero and the ratio r_∞/r_0 characterizes the effective anisotropy of the medium (often called the degree of orientation constraint) and the initial slope of r(t) gives the average velocity with which the fluorophore wobbles within a confined angle. There are several variants of this model. (1) The diffusion-in-a-cone model assumes the simplest form of the angular potential: $W(\varphi) = 0$, for $\varphi \leq \varphi_{\max}$, and $W(\varphi) = \infty$, for $\varphi > \varphi_{\max}$. This model has been applied to three types of fluorophores: (a) rod-shaped rotors with emission transition dipole moment parallel to the symmetry axis (wobbling-in-a-cone model), (b) rod-shaped rotors with emission transition dipole moment perpendicular to the symmetry axis (spinning-in-an-equatorial-band model), and (c) disk-shaped molecules with absorption and emission transition dipole moments in the plane of the disk, which undergo free in-plane rotation and restricted out-of-plane rotation.

In his later work, Kinoshita et al. extended the model by assuming Gaussian distribution of the probe orientations before the excitation with respect to the bilayer [116]. The authors compared the theoretical predictions of the Gaussian model with the original model and concluded that, if only two parameters are used, the details of the microscopic description do not have a decisive impact on the quality of the predicted fits. Lipari et al. [117] generalized the approach proposed by Kinosita by taking into account segmental motion of the lipid molecules and

assuming that the individual internal modes of motion are independent. The authors presented a model-independent equation for the residual anisotropy, r_∞

$$r_\infty = \frac{2}{5} P_2(\cos\varphi_A)\, P_2(\cos\varphi_E) S^2 \tag{30}$$

where $S = \langle P_2(\cos\varphi)\rangle$ is the order parameter, φ is the variable angle between the symmetry axis of the fluorophore and the perpendicular line to the bilayer plane, φ_A and φ_E are the angles between the absorption and emission dipole moments, respectively, and the fluorophore symmetry axis, P_2 is the second-order Legendre polynomial, and the brackets denote ensemble averaging.

At present, there are a number of models differing in the detailed description of various flexible fluorescent molecules and systems with complex relaxations or fluorophores embedded in heterogeneous media. We will not go into greater detail and will give only one example of generic complications that can occur if the polarity-dependent fluorophore is embedded in a micro-heterogeneous environment. A typical example is an amphiphilic polarity-dependent fluorophore, partially bound to polymeric micelles and partially dissolved in an aqueous medium [118]. Free probes (component 1) dissolved in an aqueous solvent (molar fraction x_1) experience high rotational mobility (their rotational correlation time is short) and their fluorescence, $F_1(t)$, is partly quenched by interaction with the polar environment (i.e., the fluorescence lifetime is short). The probes (2) bound to polymeric nanoparticles (molar fraction $x_2 = 1–x_1$, fluorescence intensity $F_2(t)$) "feel" a more hydrophobic environment (their lifetime is long) and their rotation is slow and hindered. The average fluorescence anisotropy, $r(t)$, is weighted by the fractional fluorescence intensities:

$$r(t) = \frac{x_1 r_1(t)\, F_1(t) + x_2\, r_2(t)\, F_2(t)}{x_1 F_1(t) + x_2 F_2(t)} \tag{31}$$

At short times, the fluorescence contribution of fast-emitting probes (proportional to the number of photons emitted per unit time) is important and generates a considerable weighting factor for the fast anisotropy decay, $r_1(t)$. Therefore, the overall anisotropy $r(t)$ decays quite rapidly to relatively low values at early times. At later times, the fluorescence $F_1(t)$ (not anisotropy) drops almost to zero, but $F_2(t)$ is still important. The average anisotropy starts to increase at intermediate times when $F_1(t)$ and $F_2(t)$ are comparable and passes through a local maximum when $F_1(t)$ is weaker than $F_2(t)$. At long times, only a slow anisotropy decay $r_2(t)$ is observed because $F_2(t)$ decays slowly and is still measurable, while $F_1(t)$ is practically zero. An example of complex anisotropy decay caused by the time-dependent variable weighting of the anisotropy contributions is depicted in Fig. 8. The figure shows results of fluorescence anisotropy measurements for high-molar-mass diblock copolymer polystyrene-*block*-poly(methacrylic acid) tagged by a low fraction of 2-vinylnaphthalene (on average less than one fluorophore per chain).

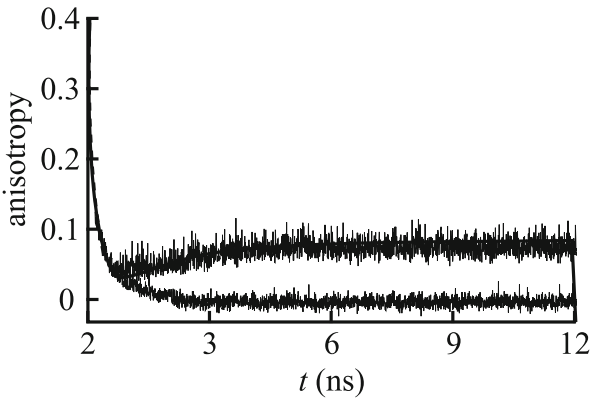

Fig. 8 Complex anisotropy decay (the *upper curve*) in a system containing two types of chemically identical probes differing in fluorescence lifetime and in mobility (as a result of different interaction with the microenvironment) compared with a simple one for a system with equivalent probes (the *bottom curve* decaying fast to zero). Adapted from Springer, Journal of Fluorescence 4, 1994, 353–356, figure 1, [118]. Copyright 1994. With kind permission from Springer Science and Business Media

The copolymer was dissolved (1) in a good common solvent of both blocks (1,4-dioxane)—monotonous curve decaying fast to zero, and (2) in a 1,4-dioxane-methanol (73 vol.%), which is a selective solvent for poly(methacrylic acid). In the selective solvent, the multimolecular micelles are formed and pendant naphthalenes are trapped in their compact and nonpolar polystyrene cores. However, the micelles coexist in mobile equilibrium with a low fraction of non-micellized unimer chains. Therefore, some pendant fluorophores are exposed to a fairly polar solvent mixture and undergo fairly fast motion. The curve measured for micellar systems has a complex shape, because it reflects the presence of two types of probes that differ both in fluorescence lifetime and in mobility. Comment: in the studied micellar system, the tagged chains were co-micellized with virtually identical non-tagged chains to lower the content of naphthalene and suppress potential complicating effects due to excitation energy migration in micelle cores. Because the rotation of micelles is much slower than the fluorescence decay, the anisotropy curve does not drop to zero on the timescale of the measurement.

11 Excimers and Exciplexes

Excimers are short-lived (transient) excited dimers formed by the bimolecular reaction of one excited fluorescent monomer (M^*) and one ground-state monomer (M) upon excitation of a low fraction of monomers. They exhibit strong fluorescence, which is red shifted with respect to that of the monomer. The main difference between excimers and excited dimers formed in the ground state prior to the

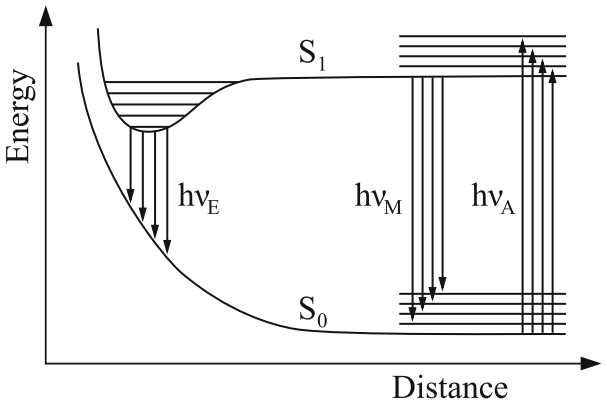

Fig. 9 The scheme of energy levels of the excited monomer and excimer as functions of the distance between the excited and ground-state monomers

excitation consists in the fact that the monomers involved in excimers do not form dimers in the ground state. Excimer formation assumes that one of the ground-state monomers, which are present in excess in the system and undergo random self-diffusion, comes close enough to the excited monomer (fluorophore) before the excited species becomes de-excited. Typical distances between molecules needed for the excimer formation are ca. 0.3 nm. It is obvious that excimers form easily in relatively concentrated solutions of fluorophores with long lifetimes of the excited state. Because the concentration of excited species is very low and there is no energy barrier on the excited energy landscape which could hinder (slow down) the formation of excimers, the reaction rate is controlled by the random self-diffusion of ground-state fluorophores. The formation of excimers can be described by the stoichiometric equation

$$M^* + M^\circ \rightleftharpoons D^* \tag{32}$$

The scheme of energy levels as functions of the distance between the monomers is shown in Fig. 9. The ground state is a purely repulsive state, i.e., at short distances, the interaction energy of two monomers decreases monotonously and steeply with their distance. The excited state exhibits a fairly deep minimum with a distinct vibrational structure. The stabilization energy is usually quite large and the red shift in the emission wavelength of the excimer with respect to the monomer fluorescence can be as large as 100 nm (e.g., for naphthalene or pyrene). The potential well of the exited dimer is smooth and relatively broad—it spans several tenths of nm and the repulsive ground-state energy changes considerably in this region. Therefore, the red-shifted excimer emission spectrum is broad. In spite of the fact that the excimer has distinct vibrational structure, its emission band is featureless without any structure, because the dimer dissociates instantaneously after the emission of a photon.

Figure 10 depicts the steady-state emission spectra of pyrene dissolved in 1,4-dioxane (normalized to the allowed third vibrational band in the monomer spectrum) for increasing concentrations. The formation of excimers belongs to

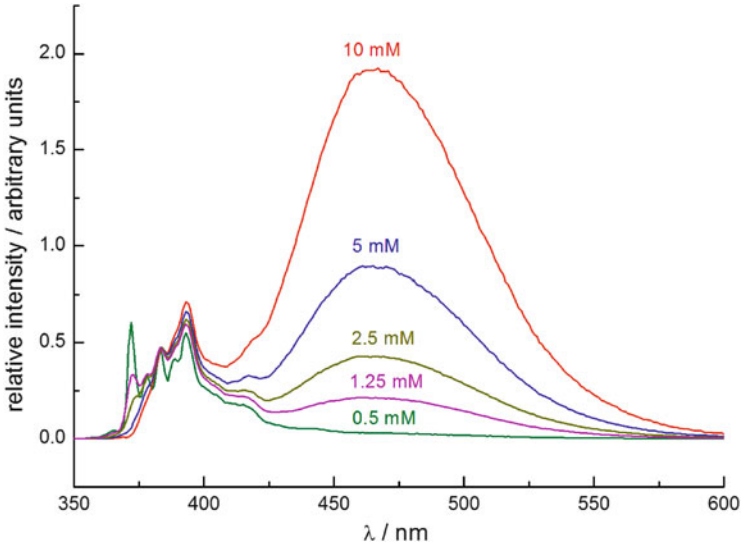

Fig. 10 Steady-state spectra depicting the pyrene excimer formation in 1,4-dioxane as a function of pyrene concentration. In case of pyrene dissolved in a fairly polar 1,4-dioxane, the I_1/I_3 ratio in pyrene monomer spectrum is higher than 1, but the excimer formation affects its value, which decreases in excimer containing solutions

the category of quenching processes (in this case self-quenching): the intensity of the monomer emission decreases and that of the excimer increases with increasing concentration of the fluorophore. Note that we present the normalized spectra (normalized to the monomer emission) and hence the monomer intensity decrease does not appear. As already mentioned, the long excited state (i.e., fluorescence) lifetime of the monomer facilitates the formation of excimers, and therefore pyrene, which has one of the longest excited state lifetimes among practically important fluorophores (more than three hundreds ns), exhibits strong excimer emission at relatively low concentrations compared with other fluorophores with shorter excited state lifetimes.

The effect of excimer kinetics on fluorescence decays of monomers and excimers upon excitation with a short pulse was studied first by Birks et al. [119]. They took into account all the relevant processes that proceed after the excitation of a low fraction of monomers by an ultrashort pulse and derived the rate equations describing the monomer and excimer decays. Most processes involved in the "Birks scheme" are monomolecular and depend only on the concentration of the excited species and on the first-order rate constant; one of them is a bimolecular process and depends on the concentrations of both the excited and ground-state molecules. They include (1) monomer fluorescence, $M^* \rightarrow M + h\nu_M$, (rate constant k_{fM}), (2) internal monomer quenching, $M^* \rightarrow M$, (k_{iM}), (3) excimer formation, $M^* + M \rightarrow D^*$ (bimolecular reaction, i.e., the rate depends on the product of the rate constant and concentration of the ground-state

monomer, c, i.e., on $k_{DM} \cdot c$), (4) excimer dissociation, $D^* \rightarrow M^* + M$, (k_{MD}), (5) excimer fluorescence, $D^* \rightarrow D + h\nu_D$, ($k_{fD}$), and (6) nonradiative excimer quenching, $D^* \rightarrow D$, (k_{iD}). To simplify the notation, they used combined parameters, $k_M = k_{fM} + k_{iM}$, $X = k_M + k_{DM} \cdot c$, $k_D = k_{fD} + k_{iD}$, and $Y = k_D + k_{MD}$. The set of differential equations that describe the reaction kinetics can be written as

$$\frac{d[M^*]}{dt} = -X[M^*] + k_{MD}[D^*] \tag{33}$$

$$\frac{d[D^*]}{dt} = -Y[D^*] + k_{DM}c[M^*] \tag{34}$$

and their solution is

$$[M^*] = \frac{[M^*]_0}{(\lambda_2 - \lambda_1)}\{(\lambda_2 - X)\exp(-\lambda_1 t) + (X - \lambda_1)\exp(-\lambda_2 t)\} \tag{35}$$

$$[D^*] = \frac{[M^*]_0 k_{DM} c}{(\lambda_2 - \lambda_1)}\{\exp(-\lambda_1 t) - \exp(-\lambda_2 t)\} \tag{36}$$

$$\lambda_{1,2} = \frac{1}{2}\left[X + Y \mp \sqrt{\left\{(X - Y)^2 + 4k_{DM}k_{MD}c\right\}}\right] \tag{37}$$

The time-resolved fluorescence intensities, $F_M(t)$ and $F_D(t)$, are proportional to the instantaneous concentrations of the excited monomers and excimers, respectively. The monomer decay is a sum of two exponentials, which means that it decreases faster than the unquenched monomer decay. The excimer is not present immediately after excitation and is formed by a diffusion-controlled process, i.e., the emission increases at early times, passes maximum, and at later times decays more slowly than the monomer fluorescence. The realistic (experimental) decays, $F_i(t)_{exp}$, are schematically shown in Fig. 11.

They are convolutions of theoretical decays, $F_i(t)_{theor}$, with the narrow pulse profile, $P(t)$, i.e.,

$$F_i(t)_{exp} = \int_0^t F_i(t^*)_{theor} P(t - t^*)dt^* \tag{38}$$

Note that, in the time-resolved measurements, the experimental monomer fluorescence decays always "copy" the excitation profile at early times and show an apparent build-up part, which is corrected and removed iteratively by the deconvolution procedure during their analysis. The relative excimer-to-monomer quantum yield, F_D/F_M, where $F_M = \int_0^\infty F_M(t)dt$ and $F_D = \int_0^\infty F_D(t)dt$, can be evaluated from the equation

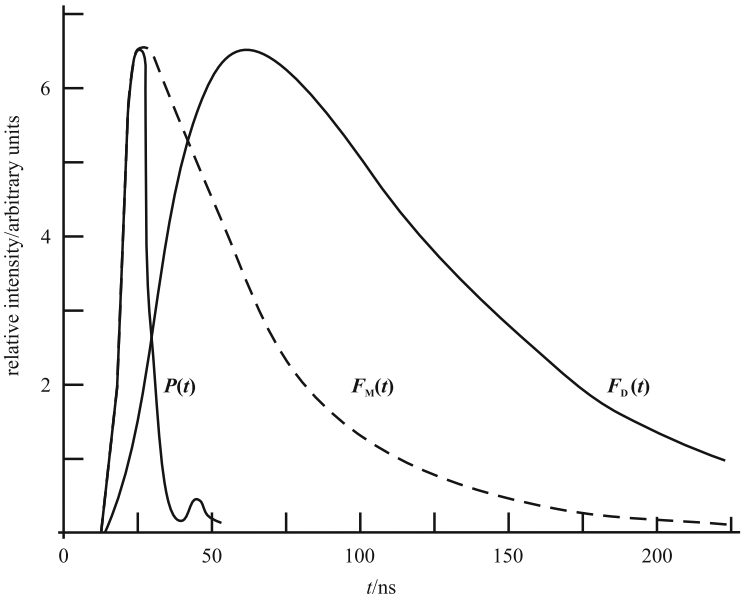

Fig. 11 The time-resolved monomer, $F_M(t)$, and excimer, $F_D(t)$, fluorescence decays calculated according to Birks scheme, taking into account the convolution of decay curves with the excitation profile, $P(t)$. Reproduced from Proceedings of the Royal Society of London Series A, Mathematical and Physical Sciences 275, 1963, 575–588, figure 1, [119]. Copyright 1963. With kind permission from The Royal Society

$$\frac{F_D}{F_M} = \frac{k_{fD}\, k_{DM}}{k_{fM}\, Y} c \tag{39}$$

Measurements of excimer kinetics are widely used fluorescence methods for studying the dynamics of multiply labeled polymer chains. For probes attached to the chain, the kinetic scheme is more complex and the resulting decays are also substantially more complicated. Because the chapter on hydrophobically modified polymers treats this topic very thoroughly, we will not go into more detail here.

Exciplexes are transient charge-transfer (CT) species formed in bimolecular quenching reactions of excited states. The chemistry and kinetics of exciplexes have been intensely studied and their role in photo-induced electron-transfer reactions has been well documented and recognized [120, 121]. One of the best studied systems is the excited complex of anthracene (acceptor) and *N*,*N*-dimethylaniline (donor). Exciplexes do not form in the ground state, but their behavior is often similar to that of excited charge-transfer complexes formed in the ground state. The properties of exciplexes are complex, because they usually reflect both the locally excited acceptor–donor state, A^*D, and the charge-transfer radical-ion state, A^-B^+. If the charge-transfer rate is predominant, the exciplex is reminiscent of the contact radical-ion pair or the solvent-separated radical-ion pair. Exciplexes play an

important role in a number of important electron-transfer processes, including processes in polymer systems [122], but this topic will not be discussed in detail here and the reader is referred to the above references and to a number of existing textbooks and excellent reviews on charge-transfer processes and on the chemistry and physics of exciplexes.

12 The Effect of Ground-State Aggregation on Fluorescence Spectra

The last part of this chapter is devoted to the general impact of weak ground-state complexation (both reversible association and irreversible aggregation) on fluorescence spectra, i.e., we will outline the spectroscopic characteristics of "J" and "H" aggregates, which are usually formed in systems of rigid planar aromatic molecules with highly delocalized π electrons, such as xanthine dyes (e.g., fluorescein) or porphyrins (see Fig. 12). As the formation of "J" and "H" aggregates occurs in a number of polymer systems (e.g., in solutions of polymeric micelles) [123] and textbook-like explanation of the principles of their formation is rare (in comparison with the literature on excimers), we will devote more space to discussion of the spectroscopic consequences of this type of aggregation. As multimolecular aggregates have been studied most frequently, we will use the term aggregation through the following text, even though the general discussion and explanation also apply to both reversible associates and dimers.

To begin with, we would like to stress once more that we will discuss the spectroscopic processes in systems of weakly bound complexes. In a number of cases, the aggregation is induced (or mediated) by interaction with the surrounding medium or with other components of the mixture. Let us give one typical example: planar fluorescent molecules are often adsorbed on surfaces (or on nanoparticles). The driving force for this process is the enthalpy of adsorption. As the concentration of adsorbed molecules increases and reaches a certain critical value, the adsorbed molecules start to repel each other. However, the repulsion between relatively large planar molecules depends sensitively on their mutual orientation and therefore the adsorbed molecules self-organize in stacks. Partially overlapping coplanar arrangement of aromatic rings relatively far from each other (ca. 1 nm) minimizes the mutual repulsion. The above example demonstrates that adsorption is a prerequisite for aggregation and that the aggregates would not form spontaneously in solutions.

Fig. 12 Porphyrins

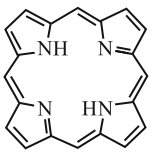

porphyrin

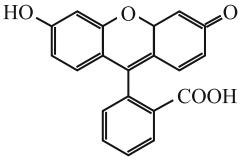

fluorescein

In contrast to excimers, the organized interacting structures are formed in the ground state and survive in the form of undissociated excited species upon excitation and the interaction of excited π^* electrons with π electrons of neighbor molecules leads to changes in their optical spectra. In 1964, Kasha [124–126] explained the changes in nondegenerate absorption bands by the exciton theory, which was originally developed by Frenkel in 1931 [127]; this theory accounts for the mutual correlation between the surplus and deficiency of negative charges in solid materials. The term "exciton" describes the bound state of an electron and an "electron hole" in supramolecular structures. It is currently used for interpretation of the optoelectronic properties of solid state materials (mainly semiconductors) and can be used to explain the spectroscopic characteristics of fluorophore crystals [128]. Kasha has shown that this concept is also applicable for small associates of two or more molecules. He mostly studied the dimers of planar aromatic molecules with transition dipole moments of both monomers lying in the same plane. In this case, the interaction strength can be characterized by the distance between the centers of gravity of the two molecules and by one angle, which describes the orientation of the dipoles with respect to the line connecting the two centers of gravity (see Fig. 13) [129].

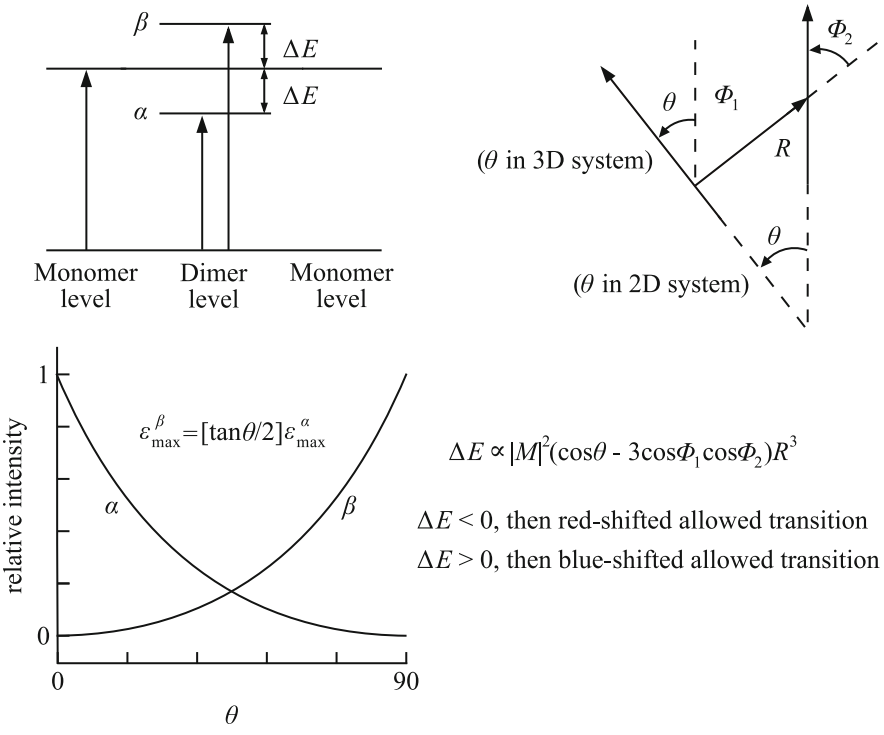

Fig. 13 Geometric and energetic scheme of formation of "J" and "H" dimers. Adapted with permission from Chemistry—a European Journal 7, 2001, 2733–273, figure 1, [129]. Copyright 2001 WILEY-VCH Verlag GmbH, Weinheim, Fed. Rep. of Germany

Efficient interaction assumes optimum approach of the two molecules and the spectral change is controlled only by one angle, θ. For a skew arrangement of the two dipole moments, the situation is more complicated and three angles, θ, ϕ_1, and ϕ_2, have to be used.

In 2D (coplanar orientation), the splitting of the excited energy levels and the spectroscopic behavior of the dimer are controlled by angle θ between the transition dipole moment and the line joining the centers of gravity of the two molecules and by their distance r. Bottom part of the figure depicts the relative intensity of transitions to the α and β states as a function of θ. In 3D (i.e., the skew arrangement), the behavior depends on three angles, θ, ϕ_1, and ϕ_2.

The interaction leads to symmetric splitting of the energy level of the π* orbitals into two different states α and β. The energy difference describing the increase (and decrease) in the states with respect to the excited monomer $|\Delta E|$is given by the following [131]:

$$|\Delta E| = \frac{\nu_2 - \nu_1}{2} \sim \frac{\left((\mu_{tr})_M\right)^2}{R^3} |\cos(\theta) + 3\sin^2(\theta/2)| \tag{40}$$

where $(\mu_{tr})_M$ is the magnitude of the transition moment of the monomer, v_2 and v_1 are the frequency maxima of the two bands α and β, and the energy difference between them is $2|\Delta E|$. The value of $(\mu_{tr})_M$ can be obtained by measuring the intensity of the monomer band, because it holds that

$$\left((\mu_{tr})_M\right)^2 = \frac{9.19 \times 10^{-39}}{\langle \nu_M \rangle} \int \varepsilon(\nu)\ d\nu \tag{41}$$

where $\varepsilon(v)$ is the absorption coefficient at frequency v and $\langle v_M \rangle$ is the average frequency of the monomer absorption band. If $\theta < 54.7°$ (lower than the magic angle), dimers or aggregates of the "J" type are formed. If $\theta > 54.7°$, dimers or aggregates of the "H" type are formed. The spectral characteristics of the two types of aggregates differ considerably [130, 131].

The extreme (limiting) arrangement of the "J" dimer is the linear "head-to-tail" arrangement with $\theta = 0°$. In this case, the transition dipole moment is parallel to the line joining the centers of gravity of the two molecules and equals $(\mu_{tr})_{DJ} = \sqrt{2} \cdot (\mu_{tr})_M$. Only the transition (excitation) to the lower state α is allowed (red shift of the absorption band), from which a strong emission (also significantly red shifted) can proceed. For the "H" dimer, the extreme (limiting) arrangement is the coplanar "face-to-face" arrangement with $\theta = 90°$ (aromatic cycles usually form this type of associates). The resulting dipole moment has the same magnitude as in the previous case, i.e., $(\mu_{tr})_{DH} = \sqrt{2} \cdot (\mu_{tr})_M$, but it is perpendicular to the line connecting the two centers of gravity. In this case, only excitation to the higher state β is allowed, i.e., we see only one blue-shifted band in the absorption spectrum. The splitting of the energy levels is usually higher because the parallel arrangement allows closer approach of the fluorophores and stronger interaction. The theory predicts

that the absorption band of the "H" dimer is broader than that of the monomer and depends on the number of aggregated monomers *n,* i.e., its half-width is $\Delta\lambda_{1/2} = (\sqrt{n})(\Delta\lambda_{1/2})_{\mathrm{M}}$. Radiative transition to the ground state is theoretically allowed but, after the absorption of a photon, very rapid nonradiative transition to the lower α state proceeds on an approx. three orders of magnitude faster timescale (than the emission), from which the radiative transition is forbidden. This actually means that the excess energy is dissipated by a cascade of nonradiative processes and "H" dimers are effectively nonfluorescent species.

However, not all fluorophores form the above-described extreme (limiting) associates. Aromatic molecules with lower symmetry (which do not have a symmetry plane perpendicular to the aromatic ring) usually form both types of associates, but the transition moments form a general angle θ with the joint line of the centers of gravity. In this case, the resulting transition moment can be decomposed into two components—parallel and perpendicular to the joining line. Both transitions (excitations from the ground state to the α and β states) are partly allowed, but the blue-shifted absorption bands is more intense than the red-shifted one in "H" aggregates and the opposite is true in "J" aggregates. In general, a relatively weak fluorescence from "H" aggregates can also occur. If the absorption bands are sufficiently separated and allow reasonable spectral decomposition, then angle θ can be estimated from spectra, because it holds that [132, 133]:

$$\tan^2\left(\frac{\theta}{2}\right) = \left(\frac{(\mu_{\mathrm{tr}})_2}{(\mu_{\mathrm{tr}})_1}\right)^2 = \frac{B_2/B_1}{\langle\nu_2\rangle/\langle\nu_1\rangle} \tag{42}$$

where $(\mu_{\mathrm{tr}})_2$ a $(\mu_{\mathrm{tr}})_1$ are the magnitudes of moments of transitions to the higher and lower energy states, respectively, which can be estimated from areas of bands B_2 and B_1, and the average frequencies of the absorption bands, $\langle\nu_i\rangle$ (which can be approximated by the corresponding maxima).

Because the bands are close to each other, $(\langle\nu_2\rangle/\langle\nu_1\rangle) \cong 1$, the last term (denominator) is often omitted. A number of practically important fluorophores of both the "H" and "J" types are formed, depending on the conditions. Rhodamine B forms "H" aggregates in aqueous media and "J" aggregates in solutions in aliphatic alcohols [134, 135]. Other compounds (e.g., some derivatives of porphyrins) form both types simultaneously under certain conditions, but the rates of their formation may differ considerably [136].

The impact of aggregation on porphyrin spectra in the region of the Soret band is substantially more complicated than the above-outlined scheme, because it involves double degenerate transition. Gouterman [137, 138] proposed a model which takes into account four orbitals. Two mutually perpendicular transition dipole moments are oriented in lines that connect two opposite NH groups. Ribó, Rubires et al. [129, 139] analyzed the possibilities for the formation of "H" and "J" aggregates for various porphyrin and metallo-porphyrin derivatives. They also reinvestigated and reanalyzed the published data on polymeric 10,20-poly(5,15-diaryl-Zn-porphyrines), synthesized and studied by Osuka et al. [140–142], Fig. 14. They showed that the arrangement of dipole moments depicted in upper part

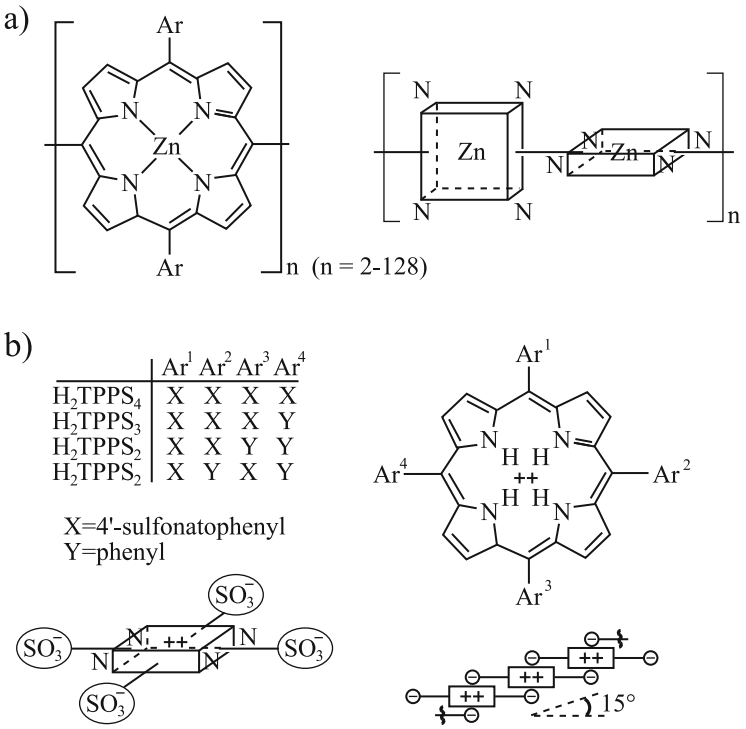

Fig. 14 (**a**) The most probable orientation of cycles in polymeric 10,20-poly(5,15-diaryl-Zn-porphyrins. (**b**) Self-assembly of anionic SO_3^- substituted porphyrins. The substituents are listed in a table which is a part of the scheme. The angle between the plane of the porphyrin skeletons and the line connecting their centers of gravity is 15°—see the *right bottom part* of the scheme. Adapted with permission from Chemistry—a European Journal 7, 2001, 2733–273, scheme 1, [129]. Copyright 2001 WILEY-VCH Verlag GmbH, Weinheim, Fed. Rep. of Germany

of Fig. 15a (symmetry group C_2) is compatible with one degenerate intense red-shifted band and one weak blue-shifted band with an intensity ratio of 3:1. The arrangement of dipole moments shown in the bottom part of Fig. 15a (symmetry group D_{2d}) yields one non-displaced absorption band (i.e., in the same position as that of the monomer) and one red-shifted nondegenerate band. The intensities of the two bands should be the same and the frequency difference between the bands depends on the degree of polymerization. The experimental spectrum agrees with the latter model, which suggests that the arrangement of dipole moments corresponds to symmetry D_{2d}. The authors also studied the spontaneous assembly of two protonated porphyrins containing four symmetrically attached negatively charged 4′-sulfonatophenyl groups [129, 139]. Taking into account strong electrostatic interactions, the most probable arrangement is that shown in Fig. 14b. The experimental value of angle α, which reflects the overlap of two coplanar planes of porphyrin skeletons, i.e., the angle between the plane defined by the porphyrin rings and the line connecting their centers of gravity, is $\alpha = 15°$.

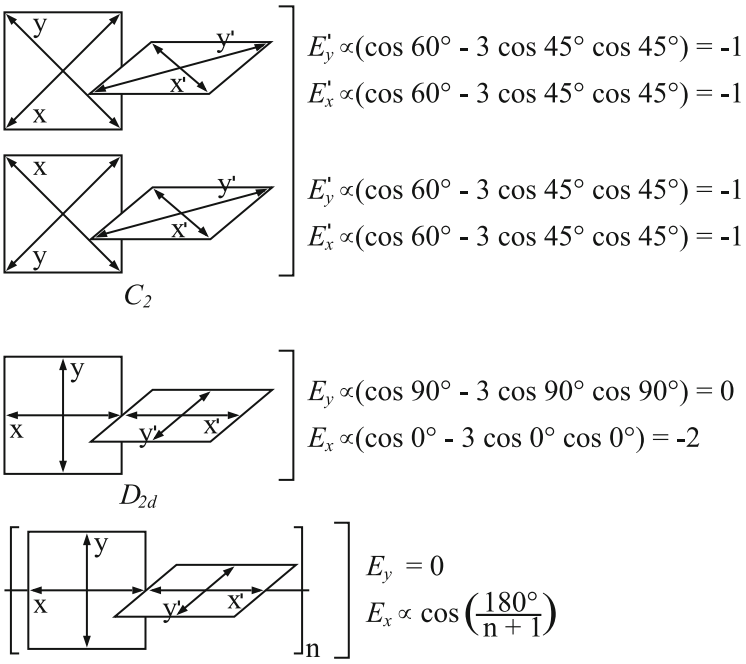

Fig. 15 (continued)

Figure 15a shows the arrangements of two porphyrin derivatives corresponding to C_2 and D_{2d} arrangements and enumerates relative changes of energy levels with respect to monomer level. The correlation diagrams in Fig. 15b depict changes in the energy levels of the excited states during gradual "insertion" of two coplanar porphyrin aromatic rings above each other as a function of angle α between the line joining the centers of gravity and the plane in which the aromatic rings lie (see the bottom right-hand side part of Fig. 14b).

Individual cases in Fig. 15b differ in the arrangement of the dipole moments with respect to each other and with respect to the direction of the "insertion." The left-hand side corresponds to "J" dimers (side-to-side π stacking) for $\alpha = 0°$ and the right-hand side corresponds to "H" dimers (face-to-face π stacking) for $\alpha = 90°$. The symmetries of all the limiting (extreme) arrangements are listed in the figure. The energies of states to which the transition is more allowed are depicted by full curves. We see that, in the first case (symmetry C_{2v} or C_{2h}), the spectrum should consist of two double degenerate red- and blue-shifted states.

In the second and third case, the spectrum should contain four nondegenerate bands. In the second case, the energy of two states should not depend on α and, in

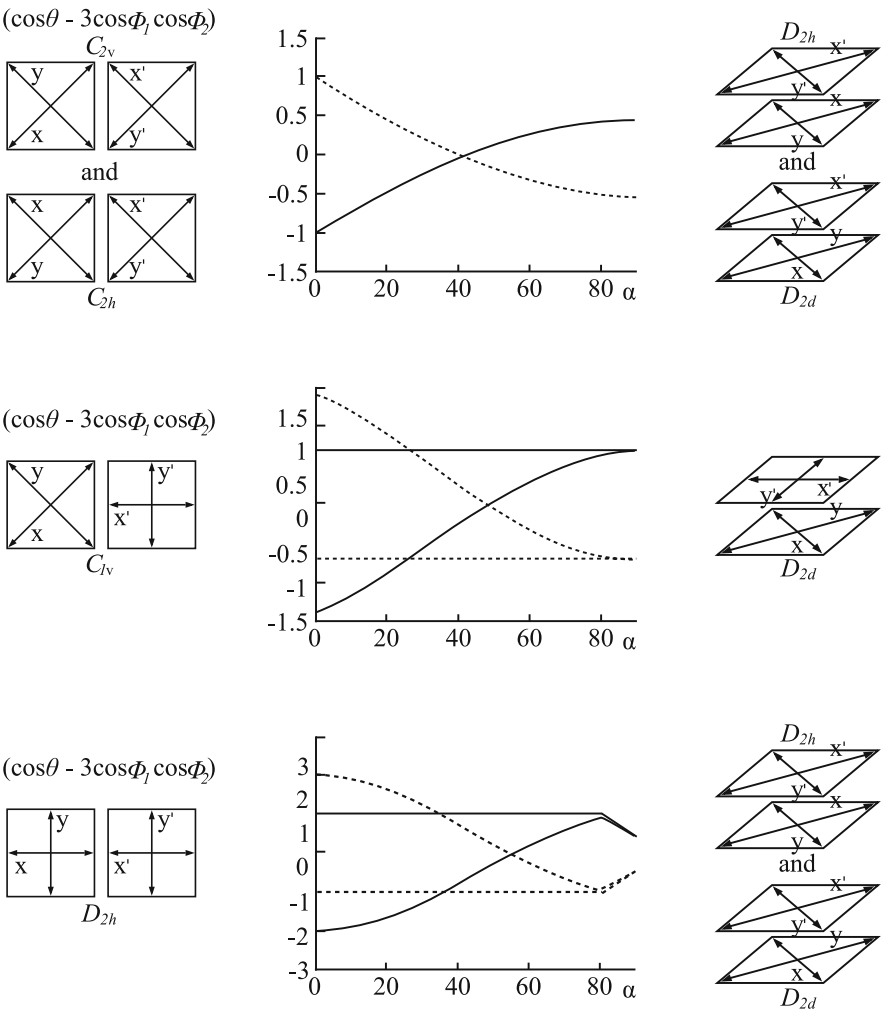

Fig. 15 (**a**) Possible arrangements of dipole moments and energy states of polymeric porphyrin derivatives (*left column*) in side-to-side arrangements (dihedral angle 90°). Relative changes of energies of possible dimer states with respect to the degenerate monomer (*right column*). The dimer yields four possible states, whose polarizations are shown in the scheme. Symmetry C_2 yields an intense degenerate red-shifted and a weak degenerate blue-shifted absorption band. Symmetry D_{2d} yields one intact (unshifted) and one red-shifted band with the same intensities. Adapted with permission from Chemistry—a European Journal 7, 2001, 2733–273, figure 3, [129]. Copyright 2001 WILEY-VCH Verlag GmbH, Weinheim, Fed. Rep. of Germany. (**b**). Correlation diagram depicting the changes in the energy of the states during the "insertion" of two coplanar aromatic porphyrin rings above each other (*middle column*), side-to-side J-arrangement, α=0° (*left column*) and face-to-face H-arrangement, α=90° (*right column*). Angle α is the angle defined by the plane of the rings and the line joining the centers of gravity of the two molecules (see the *bottom part* of the figure 14). *Full curves* depict the energy of states to which transition is allowed and the *broken curves* depict the energy of states corresponding to forbidden transitions. Adapted with permission from Chemistry—a European Journal 7, 2001, 2733–273, figure 5 [129]. Copyright 2001 WILEY-VCH Verlag GmbH, Weinheim, Fed. Rep. of Germany

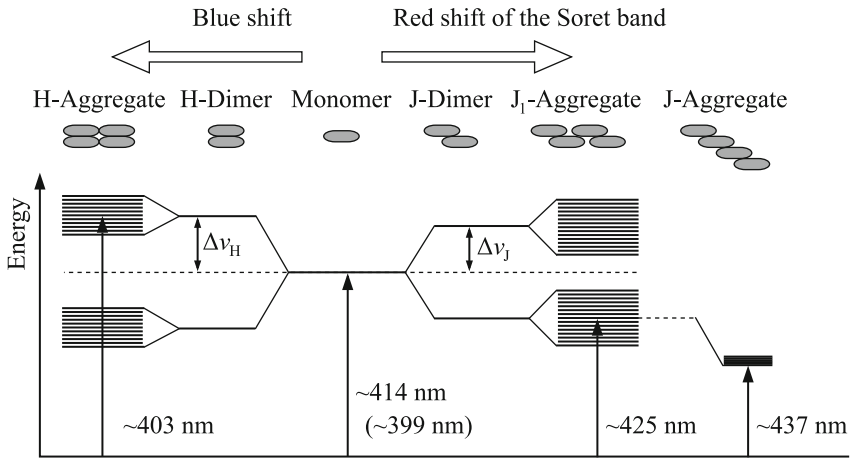

Fig. 16 Graphical summary of possible arrangements of "J" and "H" aggregates and of the corresponding energy levels. Adapted with permission from J. Phys. Org. Chem. 17, 2004, 890–897, figure 5, [143]. Copyright 2004. Wiley InterScience

the third case, it depends only in a narrow range of $\alpha \in (80–90°)$. For $\alpha = 90°$, i.e., for the face-to-face arrangement, two pairs of states become degenerate. The experimental spectrum contains only two bands, one shifted to the red and the other to the blue part of the spectrum, i.e., two degenerate bands which are compatible only with C_{2v} or C_{2h} symmetry. Evaluation of the energy split yields a fairly low angle $\alpha = 15°$, which means that the experimentally observed aggregates can be classified as "J" aggregates.

To complete the part on porphyrins, possible structures and energies of "J" and "H" associates are schematically summarized in Fig. 16.

The spectra of both "J" and "H" dimers and aggregates and the principles of their formation are now fairly well understood. Spectral decomposition enables estimation of the concentrations of the individual forms of the fluorophore in the studied system under the given conditions. However, the spectral shifts depend on the number of aggregated molecules and various spectral characteristics are often affected by slow kinetics of aggregation, which hinders the analysis.

Acknowledgment This work was supported by the Czech Science Foundation (Grants P106-13-02938S and P106-12-0143). The authors would like to thank to Lucie Suchá and Karel Šindelka for help with graphics.

Appendix: Simple Quantum Mechanics Explanation of Nondegenerate Transitions Between Energy Levels in "J" and "H" Dimers

The ground-state wave function of a dimer composed of molecules A and B, $\Psi_G = \Phi = \psi_A \psi_B$, is a totally symmetrical product with respect to all the symmetry operations of the dimer AB. The first excited state can be described by two equivalent wave functions, $\Phi_1 = \psi_A \psi_B^* \cdot \text{and} \cdot \Phi_2 = \psi_A^* \psi_B$. Their energies are degenerate. The delocalized stationary states corresponding to the "exciton," i.e., to the state in which the excited electron is not localized in any of them, are described by a symmetrical and antisymmetrical combination of the two above functions:

$$\Psi_+ = \left(1/\sqrt{2}\right)\ \left(\Phi_1 + \Phi_2\right) = \left(1/\sqrt{2}\right)\ \left(\psi_A \psi_B^* + \psi_A^* \psi_B\right) \tag{43}$$

$$\Psi_- = \left(1/\sqrt{2}\right)\ \left(\Phi_1 - \Phi_2\right) = \left(1/\sqrt{2}\right)\ \left(\psi_A \psi_B^* - \psi_A^* \psi_B\right) \tag{44}$$

The node of the wave function does not correspond to a change in the sign of the wave function, but to a change in the orientation of the dipole moment. The energies of states Ψ_+ and Ψ_- are $E \pm = \Delta E \pm E'$, where ΔE is the energy difference between the excited and ground states of the monomer and E' is the perturbation (energy splitting) due to interaction of the excited and ground-state dipoles. The value $+E'$ corresponds to Ψ_+ and similarly for –E′. This value can be calculated using the perturbation Hamiltonian and the wave functions of the unperturbed degenerate states Φ_1 and Φ_2. The perturbation Hamiltonian can be expressed as the classic expression for the energy of interacting dipoles. If we take into account only the changes in the dipoles in one dimension (which is the case for most fluorophore dimers), we can write

$$H_{\text{pert}} = \frac{e^2}{4\pi\varepsilon_0 r^3} \sum_{ij} x_A^i x_B^j \tag{45}$$

where e is the elementary charge, ε_0 is the dielectric permittivity of vacuum, and x^i describes the positions of the electrons in molecule A (x^j in molecule B).

After insertion in (45), we get

$$E' = \iint \Phi_1 \hat{H}_{\text{pert}} \Phi_2 d\tau_A d\tau_B = \frac{e^2}{4\pi\varepsilon_0 r_{AB}^3} \iint \psi_A \psi_B^* \sum_{ij} x_A^i x_B^j \psi_A^* \psi_B d\tau_A d\tau_B \tag{46}$$

Because x^i describes the positions in A only and x^j in B only, expression (44) can be rewritten

$$E' = \frac{1}{4\pi\varepsilon_0 r_{AB}^3}\left[\int \psi_A \sum ex_A^i \psi_A^* d\tau_A\right]\left[\int \psi_B \sum ex_B^j \psi_B^* d\tau_B\right] = \frac{1}{4\pi\varepsilon_0 r_{AB}^3}\vec{\mu}_A \ \vec{\mu}_B \tag{47}$$

where $\vec{\mu}_A$ and $\vec{\mu}_B$ are the transition moments of the individual molecules. The transition moments of the dimer are

$$\vec{\mu}_+ = \iint \Psi_G(\vec{\mu}_A + \vec{\mu}_B)\Psi_+ d\tau_A d\tau_B \tag{48}$$

$$\vec{\mu}_- = \iint \Psi_G(\vec{\mu}_A + \vec{\mu}_B)\Psi_- d\tau_A d\tau_B \tag{49}$$

After the insertion of the expressions for the wave functions and application of the orthogonality properties of the wave functions of different states of the same molecule, we get

$$\vec{\mu}_+ = \left(\tfrac{1}{\sqrt{2}}\right)(\vec{\mu}_A + \vec{\mu}_B) \tag{50}$$

$$\vec{\mu}_- = \left(\tfrac{1}{\sqrt{2}}\right)(\vec{\mu}_A - \vec{\mu}_B) \tag{51}$$

The above-outlined simple theoretical description provides a clue to deciding which transition is allowed and which is forbidden. For a coplanar arrangement of two aromatic rings with both dipole moments oriented in the same direction, energy contribution E' is positive, Eq. (47). State Ψ_+ has higher energy than Ψ_- and also than the excited state of the monomer. The transition moment for transition $\Psi_G \rightarrow \Psi_+$ is $\vec{\mu}_+ = \left(\tfrac{1}{\sqrt{2}}\right)(2\vec{\mu}_A) \neq 0$ and this transition is allowed. Transition $\Psi_G \rightarrow \Psi_-$ is forbidden because $\vec{\mu}_- = 0$. If the dipole moments are antiparallel, E' is negative. This means that Ψ_+ has lower energy and that transition $\Psi_G \rightarrow \Psi_+$ is forbidden because the two contributions to the final dipole moment cancel each other. It follows that the absorption spectra are identical in the two cases. Using analogous qualitative analysis for the orientation of aromatic rings in one plane, we can find that, for the "head-to-tail" as well as the "head-to-head" orientation of the dipole moments, the allowed transition will be the excitation to the lower excited state. The energy of the lower state will be the same in both cases and the dimers will be strongly fluorescent species.

References

1. Jablonski A (1935) Über den Mechanismus der Photolumineszenz von Farbstoffphosphoren. Zeitschrift für Physik 94:9
2. Prochazka K, Limpouchova Z, Uhlik F, Kosovan P, Matejicek P, Stepanek M, Uchman M, Kuldova J, Sachl R, Humpolickova J, Hof M, Muller A, Borisov O (2011) Fluorescence spectroscopy as a tool for investigating the self-organized polyelectrolyte systems. Self Organ Nanostruct Amphiphilic Block Copolym I 241:187–249. doi:10.1007/12_2010_56
3. Turro NJ, Ramamurthy V, Scaiano JC (2009) Principles of molecular photochemistry: an introduction. University Science, Sausalito
4. Guillet J (1987) Polymer photophysics and photochemistry: an introduction to the study of photoprocesses in macromolecules. CUP, Cambridge
5. Fleming G (1986) Chemical applications of ultrafast spectroscopy. Oxford University Press, Oxford
6. Franck J, Dymond EG (1926) Elementary processes of photochemical reactions. Trans Faraday Soc 21:536–542. doi:10.1039/TF9262100536
7. Condon E (1926) A theory of intensity distribution in band systems. Phys Rev 28 (6):1182–1201
8. Lakowicz JR, Masters BR (2008) Principles of fluorescence spectroscopy. J Biomed Opt 13 (2):9901
9. Beer M, Longuethiggins HC (1955) Anomalous light emission of azulene. J Chem Phys 23 (8):1390–1391. doi:10.1063/1.1742314
10. Winnik MA (1986) Photophysical and photochemical tools in polymer science. Springer, New York
11. Doi M, See H (1996) Introduction to polymer physics. Clarendon Press Oxford
12. Michl J, Bonačić-Koutecký V (1990) Electronic aspects of organic photochemistry. Wiley, New York
13. Kasha M (1952) Collisional perturbation of spin-orbital coupling and the mechanism of fluorescence quenching—a visual demonstration of the perturbation. J Chem Phys 20 (1):71–74. doi:10.1063/1.1700199
14. Stern O, Volmer M (1919) The extinction period of fluorescence. Phys Z 20:183–188
15. Lakowicz, J. (1983) Principles of Fluoresence Spectroscopy, Plenum Press, New York, NY
16. Forster T (1949) Experimentelle und theoretische untersuchung des zwischenmolekularen ubergangs von elektronenanregungsenergie. Z Naturforsch Sect A A J Phys Sci 4(5):321–327
17. Forster T (1959) 10th spiers memorial lecture—transfer mechanisms of electronic excitation. Discuss Faraday Soc 27:7–17
18. Van Der Meer W, Coker G, Chen S-YS (1994) Resonance energy transfer: theory and data. VCH, New York
19. Haan SW, Zwanzig R (1978) Forster migration of electronic excitation between randomly distributed molecules. J Chem Phys 68(4):1879–1883. doi:10.1063/1.435913
20. Ediger MD, Domingue RP, Fayer MD (1984) Picosecond studies of excitation transport in a finite volume—the clustered transport-system octadecyl rhodamine-b in triton x-100 micelles. J Chem Phys 80(3):1246–1253. doi:10.1063/1.446802
21. Ediger MD, Fayer MD (1984) Electronic excitation transport in disordered finite volume systems. J Phys Chem 88(25):6108–6116. doi:10.1021/j150669a012
22. Ediger MD, Fayer MD (1983) Electronic excited-state transport among molecules distributed randomly in a finite volume. J Chem Phys 78(5):2518–2524. doi:10.1063/1.445003
23. Farinha JPS, Spiro JG, Winnik MA (2004) Dipole–dipole electronic energy transfer: fluorescence decay functions for arbitrary distributions of donors and acceptors in systems with cylindrical symmetry. J Phys Chem B 108(42):16392–16400. doi:10.1021/jp048807
24. Yekta A, Winnik MA, Farinha JPS, Martinho JMG (1997) Dipole–dipole electronic energy transfer. Fluorescence decay functions for arbitrary distributions of donors and acceptors.

2. Systems with spherical symmetry. J Phys Chem A 101(10):1787–1792. doi:10.1021/jp9633963
25. Tcherkasskaya O, Spiro JG, Ni SR, Winnik MA (1996) Energy transfer in restricted geometry: polyisoprene-poly(methyl methacrylate) block copolymer interfaces. J Phys Chem 100 (17):7114–7121. doi:10.1021/jp9522021
26. Morawetz H (1999) On the versatility of fluorescence techniques in polymer research. J Polym Sci Part A Polym Chem 37(12):1725–1735. doi:10.1002/(sici)1099-0518(19990615)37:12<1725::aid-pola1>3.0.co;2-d
27. Chen CT, Morawetz H (1989) Characterization of polymer miscibility by fluorescence techniques—blends of styrene copolymers carrying hydrogen-bond donors with polymethacrylates. Macromolecules 22(1):159–164. doi:10.1021/ma00191a031
28. Matejicek P, Uhlik F, Limpouchova Z, Prochazka K, Tuzar Z, Webber S (2002) Experimental study of hydrophobically modified amphiphilic block copolymer micelles using light scattering and nonradiative excitation energy transfer. Macromolecules 35(25):9487–9496. doi:10.1021/ma012074g
29. Uhlik F, Limpouchova Z, Jelinek K, Prochazka K (2003) A Monte Carlo study of shells of hydrophobically modified amphiphilic copolymer micelles in polar solvents. J Chem Phys 118(24):11258–11264. doi:10.1063/1.1575732
30. Matejicek P, Podhajecka K, Humpolickova J, Uhlik F, Jelinek K, Limpouchova Z, Prochazka K, Spirkova M (2004) Polyelectrolyte behavior of polystyrene-block-poly (methacrylic acid) micelles in aqueous solutions at low ionic strength. Macromolecules 37 (26):10141–10154. doi:10.1021/ma049258q
31. Soleimani M, Haley JC, Majonis D, Guerin G, Lau W, Winnik MA (2011) Smart polymer nanoparticles designed for environmentally compliant coatings. J Am Chem Soc 133 (29):11299–11307. doi:10.1021/ja203080p
32. Uhlik F, Limpouchova Z, Matejicek P, Prochazka K, Tuzar Z, Webber SE (2002) Nonradiative excitation energy transfer in hydrophobically modified amphiphilic block copolymer micelles: theoretical model and Monte Carlo simulations. Macromolecules 35 (25):9497–9505. doi:10.1021/ma012073o
33. Limpouchova Z, Prochazka K (1994) A Monte-Carlo study of insoluble block orientations in swollen cores of multimolecular block-copolymer micelles. Collect Czech Chem Commun 59(4):803–819. doi:10.1135/cccc19940803
34. Viduna D, Limpouchova Z, Prochazka K (1997) Conformations of self-avoiding tethered chains and nonradiative energy transfer and migration in dense and constrained systems. A model for cores of polymeric micelles. Macromolecules 30(23):7263–7272. doi:10.1021/ma970002c
35. Chakrabarty D, Chakraborty A, Seth D, Sarkar N (2005) Effect of water, methanol, and acetonitrile on solvent relaxation and rotational relaxation of coumarin 153 in neat 1-hexyl-3-methylimidazolium hexafluorophosphate. J Phys Chem A 109(9):1764–1769. doi:10.1021/jp0460339
36. Brown R, Middelhoek R, Glasbeek M (1999) Solvation dynamics of fluoroprobe in diethylether. J Chem Phys 111(8):3616–3622. doi:10.1063/1.479641
37. Middelhoek ER, Vandermeulen P, Verhoeven JW, Glasbeek M (1995) Picosecond time-dependent stokes shift studies of fluoroprobe in liquid solution. Chem Phys 198(3):373–380. doi:10.1016/0301-0104(95)00219-e
38. Rosenthal SJ, Jimenez R, Fleming GR, Kumar PV, Maroncelli M (1994) Solvation dynamics in methanol—experimental and molecular-dynamics simulation studies. J Mol Liq 60 (1–3):25–56. doi:10.1016/0167-7322(94)00738-1
39. Jimenez R, Fleming GR, Kumar PV, Maroncelli M (1994) Femtosecond solvation dynamics of water. Nature 369(6480):471–473. doi:10.1038/369471a0
40. Cichos F, Willert A, Rempel U, vonBorczyskowski C (1997) Solvation dynamics in mixtures of polar and nonpolar solvents. J Phys Chem A 101(44):8179–8185. doi:10.1021/jp9716694

41. Molotsky T, Huppert D (2003) Solvation statics and dynamics of coumarin 153 in dioxane-water solvent mixtures. J Phys Chem A 107(41):8449–8457. doi:10.1021/jp034760i
42. Das SK, Sahu PK, Sarkar M (2013) Probing the microscopic aspects of 1-butyl-3-methylimidazolium trifluoroacetate ionic liquid and its mixture with water and methanol: a photophysical and theoretical (DFT) study. J Fluoresc 23(6):1217–1227. doi:10.1007/s10895-013-1252-4
43. Das SK, Sarkar M (2012) Steady-state and time-resolved fluorescence behavior of coumarin-153 in a hydrophobic ionic liquid and ionic liquid-toluene mixture. J Mol Liq 165:38–43. doi:10.1016/j.molliq.2011.10.004
44. Lippert E (1957) Spektroskopische Bestimmung des Dipolmomentes aromatischer Verbindungen im ersten angeregten Singulettzustand. Z Elektrochem 61(8):962–975. doi:10.1002/bbpc.19570610819
45. Fee RS, Maroncelli M (1994) Estimating the time-zero spectrum in time-resolved emission measurements of solvation dynamics. Chem Phys 183(2–3):235–247. doi:10.1016/0301-0104(94)00019-0
46. Mukherjee S, Sahu K, Roy D, Mondal SK, Bhattacharyya K (2004) Solvation dynamics of 4-aminophthalimide in dioxane-water mixture. Chem Phys Lett 384(1–3):128–133. doi:10.1016/j.cplett.2003.11.098
47. Chee CK, Hunt BJ, Rimmer S, Soutar I, Swanson L (2011) Time-resolved fluorescence anisotropy studies of the cononsolvency of poly(N-isopropyl acrylamide) in mixtures of methanol and water. Soft Matter 7(3):1176–1184. doi:10.1039/c0sm00836b
48. Badea MG, Detoma RP, Brand L (1978) Nanosecond relaxation processes in liposomes. Biophys J 24(1):197–212
49. Chattopadhyay A, Mukherjee S (1993) Fluorophore environments in membrane-bound probes—a red edge excitation shift study. Biochemistry 32(14):3804–3811. doi:10.1021/bi00065a037
50. Hutterer R, Schneider FW, Lanig H, Hof M (1997) Solvent relaxation behaviour of n-anthroyloxy fatty acids in PC-vesicles and paraffin oil: a time-resolved emission spectra study. Biochim Biophys Acta Biomembr 1323(2):195–207. doi:10.1016/s0005-2736(96)00186-1
51. Gafni A, Detoma RP, Manrow RE, Brand L (1977) Nanosecond decay studies of a fluorescence probe bound to apomyoglobin. Biophys J 17(2):155–168
52. Toptygin D, Gronenborn AM, Brand L (2006) Nanosecond relaxation dynamics of protein GB1 identified by the time-dependent red shift in the fluorescence of tryptophan and 5-fluorotryptophan. J Phys Chem B 110(51):26292–26302. doi:10.1021/jp064528n
53. Brauns EB, Madaras ML, Coleman RS, Murphy CJ, Berg MA (1999) Measurement of local DNA reorganization on the picosecond and nanosecond time scales. J Am Chem Soc 121(50):11644–11649. doi:10.1021/ja992456q
54. Bagchi B, Jana B (2010) Solvation dynamics in dipolar liquids. Chem Soc Rev 39(6):1936–1954. doi:10.1039/b902048a
55. Sachl R, Stepanek M, Prochazka K, Humpolickova J, Hof M (2008) Fluorescence study of the solvation of fluorescent probes prodan and laurdan in poly(epsilon-caprolactone)-block-poly(ethylene oxide) vesicles in aqueous solutions with tetrahydrofurane. Langmuir 24(1):288–295. doi:10.1021/la702277t
56. Humpolickova J, Stepanek M, Prochazka K, Hof M (2005) Solvent relaxation study of pH-dependent hydration of poly(oxyethylene) shells in polystyrene-block-poly(2-vinylpyridine)-block-poly(oxyethylene) micelles in aqueous solutions. J Phys Chem A 109(48):10803–10812. doi:10.1021/jp053348v
57. Matejicek P, Humpolickova J, Prochazka K, Tuzar Z, Spirkova M, Hof M, Webber SE (2003) Hybrid block copolymer micelles with partly hydrophobically modified polyelectrolyte shells in polar and aqueous media: experimental study using fluorescence correlation spectroscopy, time-resolved fluorescence, light scattering, and atomic force microscopy. J Phys Chem B 107(32):8232–8240. doi:10.1021/jp022221s

58. Forster S, Wenz E, Lindner P (1996) Density profile of spherical polymer brushes. Phys Rev Lett 77(1):95–98. doi:10.1103/PhysRevLett.77.95
59. Forster S, Zisenis M, Wenz E, Antonietti M (1996) Micellization of strongly segregated block copolymers. J Chem Phys 104(24):9956–9970
60. Jurkiewicz P, Sykora J, Olzynska A, Humpolickova J, Hof M (2005) Solvent relaxation in phospholipid bilayers: principles and recent applications. J Fluoresc 15(6):883–894. doi:10.1007/s10895-005-0013-4
61. Michl J, Thulstrup EW (1986) Spectroscopy with polarized light: solute alignment by photoselection, in liquid crystals, polymers, and membranes. VCH-Wiley, Deerfield Beach
62. Debye PJW (1945) Polar molecules. Dover, New York
63. Cross AJ, Fleming GR (1984) Analysis of time-resolved fluorescence anisotropy decays. Biophys J 46(1):45–56
64. Favro LD (1960) Theory of the rotational Brownian motion of a free rigid body. Phys Rev 119(1):53–62. doi:10.1103/PhysRev.119.53
65. Tao T (1969) Time-dependent fluorescence depolarization and Brownian rotational diffusion coefficients of macromolecules. Biopolymers 8(5):609–632. doi:10.1002/bip.1969.360080505
66. Ehrenber M, Rigler R (1972) Polarized fluorescence and rotational Brownian motion. Chem Phys Lett 14(5):539–544. doi:10.1016/0009-2614(72)87202-6
67. Kawski A (1993) Fluorescence anisotropy—theory and applications of rotational depolarization. Crit Rev Anal Chem 23(6):459–529. doi:10.1080/10408349308051654
68. Boens N, Novikov E, Ameloot M (2006) Compartmental modeling of the fluorescence anisotropy decay of a cylindrically symmetric Brownian rotor: identifiability analysis. Chemphyschem 7(12):2559–2566. doi:10.1002/cphc.200600309
69. Chuang TJ, Eisenthal KB (1972) Theory of fluorescence depolarization by anisotropic rotational diffusion. J Chem Phys 57(12):5094–5097. doi:10.1063/1.1678194
70. Teraoka I (2002) Polymer solutions: an introduction to physical properties. Wiley, New York
71. Rose ME (1995) Elementary theory of angular momentum. Courier Dover, New York
72. Belford GG, Belford RL, Weber G (1972) Dynamics of fluorescence polarization in macromolecules. Proc Natl Acad Sci USA 69(6):1392–1393. doi:10.1073/pnas.69.6.1392
73. Limpouchova Z, Prochazka K, Fidler V, Dvorak J, Bednar B (1993) Molecular-movements and dynamics in solutions studied by fluorescence depolarization measurement. Collect Czech Chem Commun 58(2):213–233. doi:10.1135/cccc19930213
74. Polimeno A, Saielli G, Nordio PL (1998) A diffusive model for interpreting solvation dynamics in isotropic and ordered liquid phases. Chem Phys 235(1–3):313–331. doi:10.1016/s0301-0104(98)00076-7
75. Barkley MD, Kowalczyk AA, Brand L (1981) Fluorescence decay studies of anisotropic rotations of small molecules. J Chem Phys 75(7):3581–3593. doi:10.1063/1.442468
76. Christensen RL, Drake RC, Phillips D (1986) Time-resolved fluorescence anisotropy of perylene. J Phys Chem 90(22):5960–5967. doi:10.1021/j100280a100
77. Gordon RG (1966) On rotational diffusion of molecules. J Chem Phys 44(5):1830–1836. doi:10.1063/1.1726949
78. McClung RED (1969) Rotational diffusion of spherical-top molecules in liquids. J Chem Phys 51(9):3842–3852. doi:10.1063/1.1672600
79. McClung RED (1972) Rotational diffusion of symmetric top molecules in liquids. J Chem Phys 57(12):5478–5491. doi:10.1063/1.1678249
80. St. Pierre AG, Steele WA (1972) Collisional effects upon rotational correlations of symmetric top molecules. J Chem Phys 57(11):4638–4648
81. Leicknam JC, Guissani Y (1981) On extended diffusion-models for asymmetric-top molecules in liquids. Mol Phys 42(5):1105–1120. doi:10.1080/00268978100100841
82. Fixman M, Rider K (1969) Angular relaxation of symmetrical top. J Chem Phys 51 (6):2425–2438. doi:10.1063/1.1672362

83. McClung RED (1980) The Fokker-Planck-Langevin model for rotational Brownian-motion. 1. General-theory. J Chem Phys 73(5):2435–2442. doi:10.1063/1.440394
84. McClung RED (1981) The Fokker-Planck-Langevin model for rotational Brownian-motion. 3. Symmetric top molecules. J Chem Phys 75(11):5503–5513. doi:10.1063/1.441954
85. Levi G, Marsault JP, Marsaultherail F, McClung RED (1980) The Fokker-Planck-Langevin model for rotational Brownian-motion. 2. Comparison with the extended rotational diffusion-model and with observed infrared and Raman band shapes of linear and spherical molecules in fluids. J Chem Phys 73(5):2443–2453
86. Lascombe J, Besnard M, Maraval P (1982) A new extended diffusion-model for rotational motion of symmetric-top molecules in the liquid-phase. Chem Phys 72(1–2):177–184. doi:10.1016/0301-0104(82)87078-x
87. Ghiggino K, Tan K, Phillips D (1985) Polymer photophysics. Chapman and Hall, London
88. Yip J, Duhamel J, Qiu XP, Winnik FM (2011) Long-range polymer chain dynamics of pyrene-labeled poly(N-isopropylacrylamide)s studied by fluorescence. Macromolecules 44 (13):5363–5372. doi:10.1021/ma2007865
89. Monnerie L (1991) Segmental dynamics of polymer melts. J Non Cryst Solids 131:755–765. doi:10.1016/0022-3093(91)90678-y
90. Uhlik F, Kosovan P, Limpouchova Z, Prochazka K, Borisov OV, Leermakers FAM (2014) Modeling of ionization and conformations of starlike weak polyelectrolytes. Macromolecules 47(12):4004–4016. doi:10.1021/ma500377y
91. Kosovan P, Limpouchova Z, Prochazka K (2006) Molecular dynamics simulation of time-resolved fluorescence anisotropy decays from labeled polyelectrolyte chains. Macromolecules 39(9):3458–3465. doi:10.1021/ma052557a
92. Kiserow D, Prochazka K, Ramireddy C, Tuzar Z, Munk P, Webber SE (1992) Fluorometric and quasi-elastic light-scattering study of the solubilization of nonpolar low-molar mass compounds into water-soluble block-copolymer micelles. Macromolecules 25(1):461–469. doi:10.1021/ma00027a072
93. Nagl S, Schaeferling M, Wolfbeis OS (2005) Fluorescence analysis in microarray technology. Microchim Acta 151(1–2):1–21. doi:10.1007/s00604-005-0393-9
94. Duhamel J (2014) Global analysis of fluorescence decays to probe the internal dynamics of fluorescently labeled macromolecules. Langmuir 30(9):2307–2324. doi:10.1021/la403714u
95. Duhamel J (2012) New insights in the study of pyrene excimer fluorescence to characterize macromolecules and their supramolecular assemblies in solution. Langmuir 28 (16):6527–6538. doi:10.1021/la2047646
96. Ercole F, Davis TP, Evans RA (2010) Photo-responsive systems and biomaterials: photochromic polymers, light-triggered self-assembly, surface modification, fluorescence modulation and beyond. Polym Chem 1(1):37–54. doi:10.1039/b9py00300b
97. Valeur B, Rempp P, Monnerie L (1974) Insertion of anthracene fluorophore in polystyrene chain—study of local movements via inhibition and fluorescence polarization. C R Hebd Seances Acad Sci Ser C 279(25):1009–1012
98. Valeur B, Monnerie L (1976) Dynamics of macromolecular chains. 3. Time-dependent fluorescence polarization studies of local motions of polystyrene in solution. J Polym Sci Part B Polym Phys 14(1):11–27. doi:10.1002/pol.1976.180140102
99. Viovy JL, Frank CW, Monnerie L (1985) Fluorescence anisotropy decay studies of local polymer dynamics in the melt. 2. Labeled model compounds of variable chain-length. Macromolecules 18(12):2606–2613. doi:10.1021/ma00154a042
100. Valeur B, Jarry JP, Geny F (1975) Dynamics of macromolecular chains. 1. Theory of motions on a tetrahedral lattice. J Polym Sci Part B Polym Phys 13(4):667–674. doi:10.1002/pol.1975.180130401
101. Valeur B, Monnerie L, Jarry JP (1975) Dynamics of macromolecular chains. 2. Orientation relaxation generated by elementary 3-bond motions and notion of an independent kinetic segment. J Polym Sci Part B Polym Phys 13(4):675–682. doi:10.1002/pol.1975.180130402

102. Ediger MD (1991) Time-resolved optical studies of local polymer dynamics. Annu Rev Phys Chem 42:225–250. doi:10.1146/annurev.physchem.42.1.225
103. Waldow DA, Ediger MD, Yamaguchi Y, Matsushita Y, Noda I (1991) Viscosity dependence of the local segmental dynamics of anthracene-labeled polystyrene in dilute-solution. Macromolecules 24(11):3147–3153. doi:10.1021/ma00011a018
104. Adolf DB, Ediger MD, Kitano T, Ito K (1992) Viscosity dependence of the local segmental dynamics of anthracene-labeled polyisoprene in dilute-solution. Macromolecules 25 (2):867–872. doi:10.1021/ma00028a055
105. Hall CK, Helfand E (1982) Conformational state relaxation in polymers—time-correlation functions. J Chem Phys 77(6):3275–3282. doi:10.1063/1.444204
106. Viovy JL, Monnerie L, Brochon JC (1983) Fluorescence polarization decay study of polymer dynamics—a critical discussion of models using synchrotron data. Macromolecules 16 (12):1845–1852. doi:10.1021/ma00246a009
107. Gottlieb YY, Wahl P (1963) Etude theorique de la polarisation de fluorescence des macromolecules portant un groupe emetteur mobile autour dun axe de rotation. J Chim Phys Phys Chim Biol 60(7–8):849–856
108. Burghardt TP (1983) Fluorescence depolarization by anisotropic rotational diffusion of a luminophore and its carrier molecule. J Chem Phys 78(10):5913–5919. doi:10.1063/1.444596
109. Tanaka F, Mataga N (1987) Fluorescence quenching dynamics of tryptophan in proteins—effect of internal-rotation under potential barrier. Biophys J 51(3):487–495
110. Takano T, Dickerson RE (1981) Conformation change of cytochrome-C. 1. - Ferrocytochrome-C structure refined at 1.5 A resolution. J Mol Biol 153(1):79–94. doi:10.1016/0022-2836(81)90528-3
111. Weber G (1989) Perrin revisited—parametric theory of the motional depolarization of fluorescence. J Phys Chem 93(16):6069–6073. doi:10.1021/j100353a026
112. Szabo A (1984) Theory of fluorescence depolarization in macromolecules and membranes. J Chem Phys 81(1):150–167. doi:10.1063/1.447378
113. Munishkina LA, Fink AL (2007) Fluorescence as a method to reveal structures and membrane-interactions of amyloidogenic proteins. Biochim Biophys Acta Biomembr 1768 (8):1862–1885. doi:10.1016/j.bbamem.2007.03.015
114. Lentz BR (1993) Use of fluorescent-probes to monitor molecular order and motions within liposome bilayers. Chem Phys Lipids 64(1–3):99–116. doi:10.1016/0009-3084(93)90060-g
115. Kinosita K, Kawato S, Ikegami A (1977) Theory of fluorescence polarization decay in membranes. Biophys J 20(3):289–305
116. Kinosita K, Ikegami A, Kawato S (1982) On the wobbling-in-cone analysis of fluorescence anisotropy decay. Biophys J 37(2):461–464
117. Lipari G, Szabo A (1980) Effect of librational motion on fluorescence depolarization and nuclear magnetic-resonance relaxation in macromolecules and membranes. Biophys J 30 (3):489–506
118. Procházka K, Limpouchová Z, Webber SE, Munk P (1994) Time-resolved fluorescence anisotropy measurements on fluorescently tagged amphiphilic micelles. J Fluoresc 4 (4):353–356. doi:10.1007/BF01881455
119. Birks JB, Munro IH, Dyson DJ (1963) Excimer fluorescence. 2. Lifetime studies of pyrene solutions. Proc R Soc Lond Ser A Math Phys Sci 275(1360):575–588. doi:10.1098/rspa.1963.0187
120. Gould IR, Young RH, Mueller LJ, Farid S (1994) Mechanisms of exciplex formation—roles of superexchange, solvent polarity, and driving-force for electron-transfer. J Am Chem Soc 116(18):8176–8187. doi:10.1021/ja00097a027
121. Beens H, Weller A (1975) Excited molecular π-complexes in solution. In: Birks JB (ed) Organic molecular photophysics, vol 2. Wiley, New York, pp 159–215

122. Gould IR, Young RH, Farid S (1991) Dynamics of photoinduced electron transfer in solution. In: Honda K (ed) Photochemical processes in organized molecular systems. Elsevier, New York
123. Stepanek M, Podhajecka K, Prochazka K, Teng Y, Webber SE (1999) Fluorometric and ultraviolet–visible absorption study of poly(methacrylic acid) shells of high-molar-mass block copolymer micelles. Langmuir 15(12):4185–4193. doi:10.1021/la981129d
124. Kasha M, Rawls HR, El-Bayoumi MA (1965) The exciton model in molecular spectroscopy. Pure Appl Chem 11(3–4):371–392
125. Kasha M (1976) Multiple excitation in composite molecules. In: Di Bartolo B, Pacheco D, Goldberg V (eds) Spectroscopy of the excited state, vol 12. NATO advanced study institutes series. Springer, Berlin, pp 368–368. doi:10.1007/978-1-4684-2793-6_16
126. McRae EG, Kasha M (1964) The molecular exciton model. In: Augenstein L, Mason R, Rosenberg B (eds) Physical processes in radiation biology. Academic, New York, pp 23–42
127. Frenkel JA (1931) On the transformation of light into heat in solids. II. Phys Rev 37(10):1276
128. Jelley EE (1936) Spectral absorption and fluorescence of dyes in the molecular state. Nature 138(3502):1009–1010
129. Ribo JM, Bofill JM, Crusats J, Rubires R (2001) Point-dipole approximation of the exciton coupling model versus type of bonding and of excitons in porphyrin supramolecular structures. Chemistry 7(13):2733–2737. doi:10.1002/1521-3765(20010702)7:13<2733::aid-chem2733>3.0.co;2-q
130. del Monte F, Mackenzie JD, Levy D (2000) Rhodamine fluorescent dimers adsorbed on the porous surface of silica gels. Langmuir 16(19):7377–7382. doi:10.1021/la000540+
131. Chaudhuri R, Arbeloa FL, Arbeloa IL (2000) Spectroscopic characterization of the adsorption of rhodamine 3B in hectorite. Langmuir 16(3):1285–1291. doi:10.1021/la990772c
132. Parr RG (1964) Quantum theory of molecular electronic structure. Benjamin, New York
133. Murrell JN (1971) The theory of the electronic spectra of organic molecules. Chapman and Hall, London
134. Chambers RW, Kajiwara T, Kearns DR (1974) Effect of dimer formation of electronic absorption and emission-spectra of ionic dyes—rhodamines and other common dyes. J Phys Chem 78(4):380–387. doi:10.1021/j100597a012
135. Fujii T, Nishikiori H, Tamura T (1995) Absorption-spectra of rhodamine-b dimers in dip-coated thin-films prepared by the sol-gel method. Chem Phys Lett 233(4):424–429. doi:10.1016/0009-2614(94)01477-d
136. Vergeldt FJ, Koehorst RBM, Vanhoek A, Schaafsma TJ (1995) Intramolecular interactions in the ground and excited-state of tetrakis(n-methylpyridyl)porphyrins. J Phys Chem 99 (13):4397–4405. doi:10.1021/j100013a007
137. Gouterman M (1961) Spectra of porphyrins. J Mol Spectrosc 6(1):138–163. doi:10.1016/0022-2852(61)90236-3
138. Gouterman M, Snyder LC, Wagniere GH (1963) Spectra of porphyrins. 2. 4 orbital model. J Mol Spectrosc 11(2):108–127. doi:10.1016/0022-2852(63)90011-0
139. Ribo JM, Rubires R, El-Hachemi Z, Farrera JA, Campos L, Pakhomov GL, Vendrell M (2000) Self-assembly to ordered films of the homoassociate solutions of the tetrasodium salt of 5,10,15,20-tetrakis(4-sulfonatophenyl) porphyrin dihydrochloride. Mater Sci Eng C Biomim Supramol Syst 11(2):107–115. doi:10.1016/s0928-4931(00)00147-8
140. Aratani N, Osuka A, Kim YH, Jeong DH, Kim D (2000) Extremely long, discrete meso–meso-coupled porphyrin arrays. Angew Chem Int Ed 39(8):1458–1462. doi:10.1002/(sici)1521-3773(20000417)39:8<1458::aid-anie1458>3.0.co;2-e
141. Kim YH, Jeong DH, Kim D, Jeoung SC, Cho HS, Kim SK, Aratani N, Osuka A (2001) Photophysical properties of long rod like meso–meso-linked zinc(II) porphyrins investigated by time-resolved laser spectroscopic methods. J Am Chem Soc 123(1):76–86. doi:10.1021/ja0009976

142. Osuka A, Maruyama K (1988) Synthesis of naphthalene-bridged porphyrin dimers and their orientation-dependent exciton coupling. J Am Chem Soc 110(13):4454–4456. doi:10.1021/ja00221a079
143. Prochazkova K, Zelinger Z, Lang K, Kubat P (2004) meso-Tetratolylporphyrins substituted by pyridinium groups: aggregation, photophysical properties and complexation with DNA. J Phys Org Chem 17(10):890–897. doi:10.1002/poc.783